Trends in Atmospheric Carbon Dioxide Over The Last Ten to Fifteen Years

by

Heidi Suzanne Strader

Submitted to the Department of Earth, Atmospheric, and Planetary Science
in partial fulfillment of the requirements for the degrees of

Master of Science in Meteorology

and

Bachelor of Science in Earth, Atmospheric, and Planetary Science

at the

MASSACHUSETTS INSTITUTE OF TECHNOLOGY

May 1994

Author .....
Department of Earth, Atmospheric, and Planetary Science
May 6, 1994

Certified by .....
Reginald Newell
Professor
Thesis Supervisor

Accepted by .....
Tom Jordan
Department Head

Trends in Atmospheric Carbon Dioxide Over The Last Ten to Fifteen Years

by

Heidi Suzanne Strader

Submitted to the Department of Earth, Atmospheric, and Planetary Science
on May 6, 1994, in partial fulfillment of the
requirements for the degrees of
Master of Science in Meteorology
and
Bachelor of Science in Earth, Atmospheric, and Planetary Science

Abstract

This study looks at the relative importance of the factors which control the concentration of atmospheric carbon dioxide. EOF analyses are run for both the seasonal and non-seasonal variations for the ten years from 1981 to 1990. The first seasonal EOF represents the anthropogenic component as well as the breathing of the land biosphere. Representing 85% of the variation, it has a seasonal variation of almost 6. The second shows the component of just the land biosphere and has a seasonal variation of about 4. The third seasonal EOF is thought to portray the effect of upwelling in the Eastern Pacific on the tropical strip. The first non-seasonal EOF, accounting for 97% of the total variance, shows an increase of about 11.7 for the period; that of the Northern Hemisphere is about 1.5 times that of the Southern Hemisphere.

A modification was made to the original anomalies to adjust for the long term trend in the carbon dioxide data. The rest of the procedure was the same. The first seasonal EOF, contributing to 65.8% of the variance, appears to represent changes in the NH terrestrial biosphere. The second seasonal EOF shows the variance between the long-term trend and the actual data. The third seasonal EOF, with a variance of 4, again depicts the oceanic variance due to upwelling off the coast of Peru. The first non-seasonal EOF matches the activity of the El Niño, supporting the theory that upwelling increases atmospheric CO_2 concentration. It represents over 50% of the total variation.

Error in this study may stem from unreliable station data due to infrequent sampling, not a long enough time period for the analysis, and not enough stations to develop a good global result. A stronger, standardized network would greatly enhance the outcome of this analysis.

Thesis Supervisor: Reginald Newell
Title: Professor

Acknowledgments

I would like to thank Professor Reginald Newell for all his help and understanding as my advisor. He always managed to find that one piece of information I was looking for, and also helped me through some difficult times. To Wenjie Hu, I am forever indebted for her help with my attempts to program in a language which I knew nothing about, not to mention teaching me everything she new about eigenvector analysis. No matter how matter how many times I asked, she patiently explained everything until I finally understood it.

I also want to thank my parents, Ronald and Arlene Strader, for their help and support of me in everything, no matter how small, that I have ever tried to do. They have always been there when I needed them. To my best friends Michelle Bakkila, John Hansen, Andrea Jensen, and Theresa Hutchings, I just want to say, I don't know how I could have gotten through and remained sane without you.

List of Figures

List of Tables

Chapter 1

Introduction

Carbon dioxide is an important atmospheric gas. It is responsible for absorbing and re-emitting a portion of the sun's radiation that would otherwise be reflected or re-emitted by the Earth's surface and lost to space. The fact that much of this radiation is trapped and emitted back to the surface forces surface temperatures to be higher than would otherwise be expected. In this respect, carbon dioxide is similar to atmopheric water vapor, which is the most abundant greenhouse gas in the atmosphere. Since the beginning of the Industrial Era, fossil fuel combustion has dramatically increased the amount of CO_2 in the atmosphere. Scientists have become concerned over what continued increases in atmospheric CO_2 may do to the earth's climate. Models have predicted various outcomes due to enhanced CO_2 levels. It has come to the attention of many, that the rate of increase of CO_2 in the atmosphere is not as great as calculations had predicted. Each year, only about half of the total CO_2 added to the atmosphere actually stays there. Some of the missing portion is known to be taken out by the oceans, and some by the land biosphere. However, there is still a large amount that is unaccounted for. Different arguments have been made in favor of either a terrestrial or oceanic sink, but nothing has been decisively proven.

This analysis uses an Empirical Orthogonal Function approach to look at the surface air carbon dioxide data. The EOF method separates as well as yields a rough map of the different components of variability, such as the land biosphere, the

oceanic contribution, the activity due to the El Niño, as well as other phenomena, in an attempt to distinguish their various roles. Two different sets of EOF analyses were performed. The original set up an anomaly matix directly from the raw data. However, upon inspection, it seemed that there were some discontinuities inherent in that method due to the presence of a general increase of CO_2. So, a second technique was used in which a best-fit curve was set to the raw data, and anomalies were taken from the difference between the two. This analysis produced much better results. Both of these methods include runs for the seasonal variation, and the non-seasonal variation. Such an analysis has never been done on CO_2 data before, and the hope was that it might provide a new angle in the search for the missing CO_2 sink. Both sets of results are analyzed and compared to some of the most recent theories in the literature.

Questions concerning the reliability of this analysis are discussed, as well as the accuracy of the raw data. The most important conclusion is that more stations are needed with better data sampling techniques, so that a longer, more uniform record can be put together. However, until an extensive network can be maintained and results can be collected, the quality of such analyses cannot be improved.

Chapter 2

Role of Atmospheric CO_2

2.1 Why is Atmospheric Carbon Dioxide Important?

Water vapor, carbon dioxide, and ozone are the three atmospheric gases that are most radiatively active at infrared wavelengths. They are responsible for absorbing and re-emitting heat that would otherwise be reflected or emitted by the earth's surface and subsequently lost to space. Thus the presence of these gases forces the temperature of the earth to be significantly higher than it would be without them [5]. This phenomenon is known as the "Greenhouse Effect."

Water vapor is the most abundant of these gases. The amount of water vapor an air parcel can hold depends upon its temperature. Warm air is capable of holding much more water vapor than cold air. Since temperatures are warmest near the earth's surface, and most evaporation occurs there as well, the majority of the atmosphere's water vapor is found near the surface. As height increases, the concentration of water vapor quickly falls off. Therefore, most of the contribution to infrared transfer due to water vapor is in the troposphere [1].

Ozone is primarily found in a layer in the stratosphere between 15 and 35 km [15], where it too absorbs in the infrared part of the spectrum. However, most of the focus on ozone is for its role in blocking out the harmful ultraviolet rays of the sun, and is

another topic of study in itself.

In contrast to these two gases, carbon dioxide is not concentrated in one layer. It is distributed fairly uniformly throughout the atmosphere, relatively independent of height or latitude. As can be seen from Figure B-1, carbon dioxide has a wide absorption band in the 13-18 μm region. There are also bands around 4.3 and 2.7μm, as well as several much weaker spikes, but these are not as important, since other gases such as water vapor are strong absorbers at these wavelengths. However, there is no other abundant atmospheric gas that has a strong enough band around 15μm to absorb the large portion of infrared radiation coming from the surface at those wavelengths. This radiation is then re-emitted both to space and back to the earth's surface by the carbon dioxide. Because of this absorption and subsequent re-emission of infrared radiation, the earth's surface is much warmer than it would otherwise be [7, 5].

As a result, changes in the concentration of atmospheric CO_2 have been the cause for much concern throughout the scientific community. Will a continued increase in the amount of CO_2 in the atmosphere cause temperatures to rise? Will that, in turn, cause glaciers to melt and therefore the oceans to rise? Questions such as these have instigated the creation of many models in the hopes of predicting the climate changes that may accompany the anticipated CO_2 increase.

2.2 History of Atmospheric Carbon Dioxide

The atmospheric CO_2 record can be traced back to at least 160,000 years. Data comes from analysis of gas bubbles trapped in ice cores, examination of carbonate sediments in ocean cores, and the study of carbon isotope changes found in tree rings. The best information comes from polar ice cores, where air bubbles frozen in time leave evidence of how the carbon dioxide content of the atmosphere has changed over the centuries. Figure B-2 shows a pieced together history of atmospheric CO_2. The oldest data was obtained from the core taken at Vostok, Antarctica, by the USSR. This core sample covers the time period from 160,000 to about 1,700 years Before

Present(BP). The ice core recovered at Siple Station in Antarctica provides data from 1734-1983. With this, and measurements taken at Mauna Loa, Hawaii since 1958, a fairly complete record of atmospheric carbon dioxide can be determined.

The Vostok data is shown more clearly in Figure B-3. 160,000 years ago, the concentration of atmospheric CO_2 was about 200ppmv. At about 140,000 BP, this value rapidly rose to almost 300ppmv. During the next 120,000 years, the amount of CO_2 slowly decreased back to about 200ppmv by 20,000BP. Then the concentration again increased, reaching approximately 275ppmv by 1,700 BP, the most recent part of that ice core [25].

The Siple data, shown in Figure B-4, seems to indicate that during the period from 1750 to 1800, the atmospheric concentration of carbon dioxide was fairly constant at about 280ppmv. After this pre-industrial era, the concentration began to rise at an exponential rate. By 1980, atmospheric CO_2 had reached the highest levels seen to date: around 330ppmv, and was still growing [25].

The Mauna Loa data is the longest data set to be measured in real time. That is, all carbon dioxide measurements were taken directly from the atmosphere. Measurements were started in 1958, at which time the CO_2 concentration was approximately 315ppmv. The most recent readings shown were taken in 1990, giving an average concentration of almost 354ppmv [25].

What does all this mean? Trends from 160,000 years ago may be difficult to explain exactly, but hypotheses can be made based on what we know about climate conditions at that time. For example, the low values around 30-40,000 years ago coincide with the Last Glacial Maximum. The following increase matched the glacial-Holocene transition. Ice ages and other factors, such as volcanic eruptions or variations in the solar cycle, could alter the amount of CO_2 the atmosphere holds. Volcanic activity will inject CO_2 directly into the atmosphere, while variations in the surface heating will increase or decrease ocean temperatures, thus reducing or enhancing the amount of atmospheric CO_2 that can be absorbed in the sea. What most interests scientists is the period beginning with the Industrial Era, circa 1800, to the present. In less than 200 years, the concentration has increased by approximately 70ppmv. Prior to this,

the largest increase was about 100ppmv, but over a 10,000 year period [25]! Most of this recent increase is due to combustion of fossil fuels. Each year, more and more carbon is added to the atmosphere in this manner. Each year, about 5.4 Gigatons of carbon are added to the atmosphere by fossil fuel emissions. Another 1.6 Gt comes from deforestation [16, 21]. That is, as vegetation is burned, more CO_2 is released to the atmosphere. Since there is no evidence that either of these factors will soon decrease, this rapid growth of atmospheric carbon dioxide has scientists worried over the future of climates worldwide.

2.3 What Have the Models Predicted for the Future?

Because of this concern, many General Circulation Models(GCMs) have been designed to simulate the future of the earth's climate, given different rates of change for the various gases in the atmosphere. Not surprisingly, many models have been written specifically to study how increases in CO_2 could enhance the greenhouse effect. It had been estimated that the concentration of atmospheric CO_2 would double by the year 2100, if current trends persisted. With this fact in mind, many GCMs were set up to predict what effect a doubling of CO_2 would have on temperatures worldwide.

A GCM that considers only the direct effect of increased carbon dioxide may in fact not show very much change in temperature at all. Most of the radiation escaping from the earth is emitted in the 8-13μm range, where CO_2 has no absorbing bands. The strong absorption band for CO_2 only covers the region from 13-18μm. There is already enough CO_2 in the atmosphere to absorb and re-emit all the infrared radiation leaving the earth at wavelengths corresponding to the center of this band (15μm). So the only way that enhanced CO_2 levels will directly increase the amount of radiation being trapped in the atmosphere is by increasing the radiation absorbed and re-emitted at wavelengths near the edges of this band. Since these bands are already quite strong, there is only a small growth of infrared absorption caused by the increased carbon dioxide [1].

If a GCM is to accurately consider the effect that enhanced atmospheric carbon dioxide levels will have, then certain feedbacks must be included. For example, the effect that increased CO_2 has on the water vapor content must be taken into account. Since more carbon dioxide will trap more heat, the temperature of the atmosphere will increase. This will allow more moisture to evaporate, especially near the surface, where water is plentiful. Since water vapor also acts as a greenhouse gas, as described previously, the temperature of the atmosphere will continue to increase. Warmer air is able to hold still more water vapor, so a positive feedback cycle has been created.

The planetary albedo must also be considered. If temperatures increase, then less snow and ice will be found on the surface of the earth. This decreases the planetary albedo, allowing more direct radiation to be absorbed at the surface (less reflection), which subsequently increases the temperature. This is another positive feedback cycle [16].

There are many factors which, depending on how they are included, may seriously affect the outcome of a GCM. For instance, cloud feedback can augment or diminish the effect of carbon dioxide warming. Depending on the height of the cloud, it may either trap long-wave radiation, thus enhancing the greenhouse effect, or reflect it, thereby increasing the planetary albedo and reducing the temperature. The effect of the deep oceans is another consideration. There will be a certain lag time until the concentration of CO_2 in the oceans equilibrates with that in the atmosphere. Depending on what mixing rates are used, which salinities are chosen, the wind stresses considered, and how it is decided to approximate the physical processes of the ocean, similar models can output very different results. Perhaps the most difficult factors to model are unpredictable climate forcing mechanisms. These include volcanoes, changes in ocean circulation, and other chaotic, unexpected events. Since such events are impossible to forecast and provide numerous possibilities, only a limited number of scenarios can be modelled [1].

GCMs are forced to find a compromise between simplicity and realism. In order to simulate something as realistically as possible, the model must be fairly complicated. However, if too detailed, it reaches a point where adding parameters or increasing

the number of grid points no longer improves the results. Also, in order to keep the solutions from being too case-specific, some assumptions and generalizations must be made. There is a thin line where certain factors are sacrificed and others are included to keep both the computations reasonable and the results useful.

It is easy to see that these and other factors make modelling very difficult to do. Different models have predicted temperature increases ranging from two to five degrees Celcius for a doubling of atmospheric CO_2. Early estimates were closest to five degrees, but most recent models predict anywhere from two to four degrees, depending on the parameters chosen. I won't go into detail here, but the reader can refer to [16, 1] for more information.

2.4 How Well Have the Models Simulated Observed CO_2 Changes?

In the last few years, it has been observed that the concentration of atmospheric carbon dioxide is not increasing at the rate that it was expected to. The globally averaged atmospheric CO_2 concentration has increased by about 1.22ppmv per year since the late 1970s through the 1980s. At this rate, the concentration will increase by almost 130ppmv during the next century, reaching approximately 480ppmv by the year 2100 [25]. Though this is a significant increase, it is nowhere near the doubled amount of approximately 680ppmv that was expected to have accumulated by that time [1]. Most recently, the increase in atmospheric CO_2 concentration has decreased [19]. Unfortunately, the raw data was not accessible at the time of this study. So why has the rate of CO_2 accumulation suddenly slowed down?

In making estimates of future atmospheric CO_2 concentrations, it had been assumed that as time passed, more of the carbon released to the atmosphere would stay in the air. During the 1950s, it was estimated that approximately 40-45 percent of carbon input stayed in the atmosphere. The same was true during the 1960s, at which time the measured increase of atmospheric CO_2 concentration was 0.6 to 0.7ppmv per year. By 1970, this had become almost 1.0ppmv per year [1]. As mentioned above,

however, that rate only increased to 1.22ppmv per year during the 1980s, and held fairly constant throughout that decade [25]. Most recently the rate of increase has slowed down. Meanwhile, it is still true that the portion of carbon emissions that stays in the atmosphere is still about fifty percent.

Models can be made of the amount of carbon input to the atmosphere by fossil fuel combustion fairly accurately since the amount of oil consumption can easily be monitored. The contribution by deforestation and biomass burning cannot be measured in such a manner, but can be approximated. Unfortunately, these approximations have a large error associated with them, making it difficult to determine exact values for the expected atmospheric CO_2 content. However, the models assume a certain range of values [21], which generally lead to the same questions. Why do only half of the known carbon emissions actually stay in the atmosphere? Where does the other portion go? Why has the rate of accumulation begun slowing down? It is known that some CO_2 is taken up by the oceans, and some by the terrestrial biosphere, but how much by each? But a considerable portion of the missing CO_2 is still unaccounted for. The purpose of this study is to contribute to progress in answering these questions. Possible solutions will be looked at in more detail in Chapter 6.

Chapter 3

Procedure

My research involved the use of Empirical Orthogonal Functions and eigenvector-eigenvalue analysis to examine trends in atmospheric carbon dioxide data over a ten year period. The first section provides a brief outline of the basic EOF procedure. The second section encompasses all the steps that were necessary to my research.

3.1 Empirical Orthogonal Functions

When dealing with a large data set, the total raw data may be too much information to digest. Empirical Orthogonal Function analysis, or EOF, provides a means of simplifying the data to a level that is much easier to study and understand, while retaining the maximum amount of information. This discussion is a paraphrased version of the explanation offered by Jane Hsuing in her thesis [8]. Her explanation was so well written that I could not make any improvements, nor write it any other way without losing much of the clarity that her paper exuded.

EOF begins with an ixj matrix M, where i describes the number of rows, and j the number of columns. Physically speaking, i is the number of observations at each of the j locations. We stipulate that M can be factored into two different matrices, X and Y:

$$M = XY. \tag{3.1}$$

The following conditions are imposed:

$$X^T X = D \tag{3.2}$$

$$YY^T = I \tag{3.3}$$

where X is an ixj and Y a jxj matrix. D is a diagonal jxj matrix and I is a jxj identity matrix.

Taking the transpose of each side of (3.1):

$$M^T = (XY)^T = Y^T X^T, \tag{3.4}$$

then multiplying (3.1) by (3.4):

$$M^T M = Y^T X^T XY, \tag{3.5}$$

and substituting in for D by equation (3.2) gives:

$$M^T M = Y^T DY. \tag{3.6}$$

Finally, through matrix multiplication and use of (3.3):

$$M^T MY^T = Y^T D. \tag{3.7}$$

But, $M^T M$ is simply the correlation matrix, C, as will be discussed in the next section, so (3.7) becomes:

$$CY^T = Y^T D. \tag{3.8}$$

The columns of matrix Y^T are the eigenvectors of the correlation matrix. The above equation could also be written as:

$$YC = DY. \tag{3.9}$$

where Y contains the eigenvectors arranged in rows. In both cases the diagonal elements of D define the eigenvalues for C. I prefer the column arrangement, so equation (3.8) will be used throughout the calculations.

The task of solving for the matrices Y^T and D is an eigenvector-eigenvalue analysis problem. By definition, the eigenvectors are orthonormal to one another, and so act as weighted representations of the data at different sites. Once determined, the eigenvectors provide a space component as well as a time series that shows how each vector varies over time. By looking at these instead of the original data, the problem is much simplified, and different components may be isolated and examined individually.

The different components account for different percentages of the total variation. This can be shown by the traces of our matrices. The trace of a matrix is the sum of all its diagonal elements [22]. Using some matrix algebra and equation (3.8), we can say that:

$$Tr(C) * Tr(Y^T) = Tr(Y^T) * Tr(D) \tag{3.10}$$

$$Tr(C) = Tr(D). \tag{3.11}$$

The sum of the diagonal elements of the correlation matrix is thus equal to the sum of the eigenvalues in the diagonal matrix. Since by definition, the correlation matrix is the variance-covariance matrix, then the total variance is also expressed by the sum of the eigenvalues. Each eigenvalue, in turn, represents the relative importance of its associated eigenvector in comparison to the other vectors.

The ratio r_m:

$$r_m = d_m / \sum_{m=1}^{j} d_m, \quad \text{m=1,2,3,...,j} \tag{3.12}$$

where d_m is the mth eigenvalue, expresses the percent contribution that the mth eigenvector makes toward the total variance.

The eigenvalues can be reordered from largest to smallest, as long as their associated eigenvectors are rearranged as well. This way, the largest portion of the variance is accounted for by the first eigenvector, the second largest by the second, and so on.

The first k eigenvectors will contribute

$$\sum_{m=1}^{k} r_m \tag{3.13}$$

percent of the total variance. We can choose k such that most of the total variance is explained by those k eigenvectors. This is where EOF becomes quite useful; we can look at only those k components instead of the complete set of j components and account for nearly all the variance. Exactly how many eigenvectors are significant depends on the particular set of data. If the error associated with each eigenvalue is determined, then the point at which the error bars overlap signifies that the eigenvector is in the noise level of the problem, and the results are inconclusive.

3.2 Procedure

EOF analyses were run for both the seasonal and non-seasonal case, as will be described below. The seasonal values should show only seasonal variations, with highs and lows recurring at the same time each year. The non-seasonal should remove these annual cycles, leaving only long-term fluctuations, such as changes in fossil fuel consumption, deforestation, and the El Niño. The data from seventeen different World Meteorological Organization/ Background Air Pollution Monitoring Network(WMO/BAPMoN) stations over the ten years from 1981-1990 was used. These stations and their particular characteristics are listed in Table A.1, while Figure B-6 shows their locations on a map. Observations were made using either an Infrared Continuous Analyzer, or a flask sampling method. The continuous analyzer runs all the time, thus giving quite accurate average values for each day. The flask samples are taken at intervals which vary depending on the station. Some take readings every day, while others only take several per month. Though there are other stations collecting CO_2 measurements besides these seventeen, either the observations were unreliable, too infrequent, or they were not collected over a long enough period of time. The raw data came from *Trends '91*, and was verified by the yearly *WMO Provisional Daily*

Atmospheric Carbon Dioxide Concentrations publications. It was given in the form of monthly mean surface concentration of atmospheric CO_2 in ppmv.

The first step is to create an ixj matrix A of the form:

$$A = \begin{pmatrix} a_{1,1} & a_{1,2} & \cdots & a_{1,j} \\ a_{2,1} & a_{2,2} & \cdots & a_{2,j} \\ \vdots & \vdots & & \vdots \\ a_{i,1} & a_{i,2} & \cdots & a_{i,j} \end{pmatrix}$$

In this case, there is a 120x17 matrix. Each of the 17 columns represents a different station. The 120 observations for each station are for the 120 months spanning the ten year period. Average monthly values are given in the form of total ppmv of atmospheric CO_2. However, the correlation matrix that we are trying to create requires a matrix of anomalies, not the actual concentrations. We can determine the anomalies by making the assumption that each observation can be broken down into a mean component plus some deviation from that mean:

$$x = \bar{x} + x' \tag{3.14}$$

and therefore the anomaly x':

$$x' = x - \bar{x}. \tag{3.15}$$

To solve for the seasonal anomalies, one average value for the whole time period is calculated. Setting this equal to $\bar{x}$ and implementing equation (3.15), the anomalies for each month can then be found. For the non-seasonal matrix, twelve different averages (one for each month of the year) are determined for the ten year period. Then the non-seasonal anomaly for each month is calculated using the mean value $\bar{x}$ for that month. The seasonal anomalies are put into one matrix and the non-seasonal into another. From this point the anomaly matrices are kept separate, but the procedure for both is the same.

After the anomaly matrices are set up, they have to be normalized by the standard

deviation. The standard deviation is calculated using the expression [6]:

$$\sigma_m = \sqrt{\sum_{n=1}^{i} [a_{n,m}{}^2] \,/(i-1)}, \quad \text{m=1,2,3,...,j} \tag{3.16}$$

where i is the total number of observations per station (in this case 120), and $a_{n,m}$ refers to the corresponding anomaly from the original matrix. The standard deviation anomalies must be calculated for each of the 17 stations. They can then be used to solve for the normalized anomalies of the initial matrix:

$$a'_{n,m} = a_{n,m}/\sigma_m. \tag{3.17}$$

This new matrix of normalized anomalies $a'_{n,m}$, which is still of dimension ixj, will be called M. After this normalized anomaly matrix is obtained, its transpose must be determined. The transpose of a matrix is defined by:

$$M_{n,m} = M^T{}_{m,n}. \tag{3.18}$$

Multiplying $M^T M$ gives the correlation, or variance-covariance matrix. The variance-covariance matrix is known as such because it contains time-variances for each station and the space covariance between the stations. It is a symmetric matrix that by definition contains the variance for all the observations along its diagonal [6], as was shown previously.

At this point, the eigenvectors and eigenvalues of the correlation matrix can be determined according to Section 2.1. The actual work is done by computer. Once the eigenvalues and eigenvectors are obtained, the time series and spacial maps of the vectors can be created.

The time series describing the variance of the vectors over time is calculated by multiplying the standard deviation anomaly matrix, M, by the eigenvector matrix, or:

$$T = MY^T \tag{3.19}$$

where T is an ixj matrix of the time series. Since the percentage of variation contributed by each eigenvector is known by its associated eigenvalue, only the most significant vector time series need be plotted. In this case, time series for the first three eigenvectors are shown, for both the seasonal and non-seasonal cases.

Spacial maps are drawn up by plotting each component of an eigenvector at its corresponding station. This will show where the biggest variations are coming from for a particular eigenvector. Remember, the vectors act as weights, so they will show how much influence each station has for that particular eigenvector. Again, only the three most significant eigenvectors are mapped for the seasonal and non-seasonal runs.

Because the anomalies have been divided by the standard deviation, the units have canceled, and both the eigenvectors and the time series will be non-dimensional values.

EOF analyses were run for the 17-station matrices. Subsequent runs were made dividing the stations into two hemispheres. One run looks at the 12 stations in the Northern Hemisphere, the other at the 5 in the Southern Hemisphere. The results from the two separate hemispheres can then be compared to the global analysis to see which hemisphere dominates the overall trends.

Chapter 4

Results and Discussion

4.1 Seasonal EOF

Several runs were performed using the seasonal analysis. The first was for all 17 stations, under the conditions described in the previous chapter. The next run was for only the 12 stations located in the Northern Hemisphere, and the last was for the 5 stations in the Southern Hemisphere. Trends and patterns could be evaluated, and the contribution from each hemisphere could then be assessed. The time series for the first three seasonal EOFs are shown in Figure B-7, while their eigenvectors are Figures B-8, B-9 and B-10. The time series of the seasonal EOFs for the Northern and Southern Hemisphere are seen in Figures B-11 and B-12, respectively. The eigenvector maps for the hemisphere-specific runs have been omitted since there were few stations for each and the data appeared to be inconclusive. The percent contribution for each EOF is given in Table A.2.

4.1.1 First Seasonal EOF

The first seasonal eigenvector accounts for almost 85 percent of the seasonal variance. The time series shows a seasonal peak to trough variance of 5 to 6 (in non-dimensional units as noted), and an increasing long-term trend of approximately 10.3 over the ten year period. This would indicate an increase of a little more than 1 per year during

the period from 1981 to 1990. So, the seasonal variation is about five times the magnitude of the yearly increase, or half that of the ten year trend.

This EOF appears to be the sum of the major components involved in the atmospheric carbon dioxide cycle. The long term increase is a result of the addition of anthropogenic carbon dioxide, which is primarily due to fossil fuel combustion and deforestation. The seasonal variation is dominated by the breathing of the land biosphere, with peaks in the spring and lows in the fall.[1] The seasonal signal of the land biosphere may be mixed with a seasonal variation in anthropogenic CO_2 as well. During the winter, people living in higher latitudes will burn more oil to heat homes and businesses, so it seems likely that there will be an increase in anthropogenic CO_2 emissions during this season. Since the majority of buildings with such heating will be in the Northern Hemisphere, the seasonal cycle of such a factor would maximize from December to January, and drop again during the summertime. Of course, the argument could be made that air conditioning in the summer will keep the signal fairly consistent year-round. At this point, there are no conclusive studies, and such a pattern has yet to be evidenced, but it is simply mentioned here as a possible factor in the time series of this EOF.

The eigenvector map for the first seasonal EOF, Figure B-8, shows a fairly uniform distribution corresponding to a simultaneous increase over the whole globe. There are slightly higher values in the lower and mid-latitudes of the Northern Hemisphere, suggesting that the contribution is greatest from this region. It is known that much of the seasonal variation due to the land biosphere comes from the mid-latitudes of the Northern Hemisphere,[2] which could explain the large variances found there. However, if this were the only factor, then the Northern and Southern Hemispheres should be of opposite sign, since their seasons are out of phase. Also, the lower latitude variance can't be explained by the land biosphere, since it has little seasonality at these latitudes. Therefore, it is most likely that the eigenvectors are reflecting the long-term anthropogenic effect in the lower and mid-latitudes. Most anthropogenic

[1]This pattern will be explained in Section 4.1.2, for the case of the second EOF.
[2]Also to be described in Section 4.1.2.

carbon is known to be injected into the atmosphere at Northern Hemisphere mid-latitudes, so the fact that there are higher vector values in the northern sub-tropics as well may be due to wind transport of the airborne CO_2. Therefore the seasonal variance due to the combination of anthropogenic and biospheric components is felt most strongly between 10°N and 40°N. The time series for the hemisphere-specific runs also show that the NH is dominant (see Figures B-11 and B-12 discussed below).

From the eigenvector map and the time series, it is clear that the Northern Hemisphere dominates the seasonal pattern of the first EOF. This could be due to the fact that of the 17 stations included in the analysis, 12 were from the Northern Hemisphere, giving a much larger weight to northern trends. In order to determine the contribution by the separate hemispheres, the time series for each can be examined. The first seasonal Northern Hemisphere EOF is responsible for almost 92 percent of the total variance and has a time series that is almost identical to the first global EOF described above. In Figure B-11, the variance is almost exactly the same, as well as the maximums and minimums for each cycle. The first EOF for the Southern Hemisphere, contributing over 98 percent of the variance, is of opposite phase to the Northern Hemisphere. It shows a maximum in August or September, and a minimum in March or April. This follows since the terrestrial biosphere will be flourishing in the Southern Hemisphere from August till March, using up CO_2, and will be virtually lifeless the rest of the year. However, changes in anthropogenic CO_2 could also be represented by these patterns, making it difficult to separate its contribution from that of the land biosphere. Either way, the SH variation is very small compared to the Northern Hemisphere. Its seasonal amplitude is less than 0.5, in contrast to an amplitude of 5 in the Northern Hemisphere, making the variation in the NH ten times as great. So the time series for the hemisphere-specific cases agree with the eigenvector maps from the global run, showing a smaller variation in the Southern Hemisphere. Therefore, it makes sense that most of the variance for the first seasonal EOF is due to fluctuations of the Northern Hemisphere, and the Southern Hemisphere has but a small contribution in comparison.

4.1.2 Second Seasonal EOF

The second seasonal EOF, which accounts for a little more than 11 percent of the variance, seems to have extracted the terrestrial biosphere from the curve of the first EOF. Its time series clearly shows the seasonal breathing of the land biosphere. Trees and plants require carbon dioxide for the process of photosynthesis. We see evidence of this in the spring, that as the vegetation begins to flourish, more carbon dioxide is taken out of the atmosphere. Since the spring bloom occurs rather quickly, the atmospheric decrease is quite rapid. CO_2 concentrations continue to plummet throughout the summer months, as long as green plants are able to thrive. By autumn, however, most of the leaves have fallen off the trees, depriving the atmosphere of this CO_2 sink. At this point, the now decaying plant material liberates carbon dioxide back into the atmosphere through the process of respiration. This increase occurs throughout the winter months, at a rate slower than the spring decrease. It is slower because the decay process occurs gradually, taking time to release carbon dioxide back to the atmosphere. All of these features are clearly seen in the second EOF curve, with a gradual rise always followed by a sharper drop-off.

The Northern Hemisphere dominates this seasonal pattern, with highest atmospheric concentrations of CO_2 in the NH spring, April and May, and the lowest concentrations occurring in August and September. Indeed, raw data shows that there is generally greater seasonal variation in the Northern Hemisphere. This is not surprising since there is more land mass in the Northern Hemisphere, providing a larger area for plantlife to flourish, and thus a greater terrestrial sink for CO_2 during the NH summer. The individual hemispheres will be discussed at the end of this section to determine their respective contributions to this curve.

The second EOF time series shows a smaller peak to trough variation than the first. The seasonal change is approximately 4 units. This is a large percentage of the magnitude given by the combined components in the first eigenvector. So, it would seem that the land biosphere accounts for at least two-thirds of the variability in the first eigenvector, leaving the anthropogenic component to make up the difference. What is interesting to note is that this second EOF is actually decreasing over the

ten year period by about 1.6 units. If this component does indeed represent the land biosphere, then the time series indicates that it's role is decreasing! Arguments concerning deforestation say that the area of land covered by vegetation is decreasing, particularly in the tropical rainforests, and therefore less CO_2 is being consumed by the land biosphere. If the rainforests specifically were being reduced, then the seasonal variance would increase, because with less tropical vegetation, the effects of the more variable, high-latitude forests would become more predominant in the seasonal cycle. Close examination of the time series shows that the seasonal amplitude is increasing over the ten year period, by a factor of almost 1.2. This could indeed indicate that some of the tropical rainforests are being destroyed, while simultaneously, less atmospheric CO_2 is being consumed by the land biosphere.

Figure B-9 shows the second eigenvector with negative values north of 20°N, and positive values south of that latitude. The fact that the hemispheres are of opposite sign reflects that their seasonal cycles are out of phase. It seems that the smallest eigenvectors are found in the tropics, and the largest are around 60° latitude. This corresponds with the fact that the seasonal variation of the land biosphere is much less at low latitudes, and highest at upper mid-latitudes. The large change in solar heating at higher latitudes allows plants and trees to grow during the summer months, but in the winter the biospheric activity is virtually zero. Near the Equator, the solar insolation does not change much, and plant activity stays about the same. So, this second EOF agrees with what we would expect to find if it is indeed the contribution of the land biosphere.

The EOF time series for the second eigenvector in the Northern Hemisphere again is very similar to that of the global run. The peaks and troughs occur in phase. The NH seasonal variance is only a little more than 2, as opposed to 4 in the global analysis, and its long term trend is a decrease of less than 1 over the ten year period. These values do not equal those of the total run, but they are augmented by the second seasonal EOF for the Southern Hemisphere. It is out of phase with the Northern Hemisphere, increasing from August to March, and decreasing again until August; the exact opposite of the Northern Hemisphere. The SH peak to trough variation is

difficult to determine because the curve is not even, but it varies between 0.3 and 0.5. The long term trend is approximately 0.04. So, the Northern Hemisphere appears to play the dominant role in the terrestrial biosphere, which has been anticipated from the analysis of the eigenvector maps from the global analysis.

4.1.3 Third Seasonal EOF

The third seasonal EOF time series is out of phase with the first two time series. It reaches a maximum in October, and a minimum in July. There is a peak to trough difference of approximately 2. This component of the seasonal variation is about half the magnitude of the first two EOFs. It is only responsible for about 1.5 percent of the total seasonal variance. There does not appear to be any overall increase during the ten year period.

What this time series is showing is not as easily determined as the first two. Looking at its associated eigenvector map in Figure B-10 may give some idea. All of the stations are positive except those in the region from 10°S to about 30°N. Since the map shows a differing variability in this entire tropical strip, it seemed obvious that something in this region was influencing the atmospheric CO_2. Upon looking at the average SST for the tropical strip, it became apparent that the highest temperatures were found in August and the lowest were seen in February. This seemed to be in phase with the third EOF curve. As was stated previously, more CO_2 can be taken up by colder water. So, it might seem that this is a direct effect of the solubility of CO_2 in water. when the temperature is high, the more CO_2 is forced out of the ocean and into the atmosphere. However, observations of actual ocean data can be used to refute this. In the papers by Inoue and Sugimura [10, 11], it was difficult to see a consistent relationship between sea surface temperature and pCO_2 in the water. So it would seem that this is not a strong basis on which to make a conclusion.

Instead of looking at the average sea surface temperatures for that entire strip, consider only the SST for the Eastern Pacific waters off the coast of South America. The SST in this region is shown in Figure B-13 along with the third EOF time series. The SST graph shows the monthly anomalies calculated off the yearly average, as

given in [4]. This curve is of opposite phase to the EOF. It reaches a minimum about one month before the atmospheric CO_2 concentration peaks, and a maximum three to four months before the lowest CO_2 levels are measured. So how is this eigenvector related to the SST in this narrow region?

It is known that the tropical oceans have a higher concentration of dissolved carbon dioxide than those at higher latitudes. Therefore, the oceanic pump takes up CO_2 nearer the poles, and transports it to low latitudes. After it is absorbed, the CO_2 sinks to the bottom of the ocean where dissolving $CaCO_3$ supplies additional CO_2. The concentration of CO_2 thus increases as the water is transported at great depths toward the Equator. As it nears the Equator, upwelling occurs. This cold water comes to the surface in the tropics, and liberates its excess CO_2 to the atmosphere, where it will be mixed throughout the atmosphere and can again be taken up in the cold polar regions. When the strongest upwelling takes place, the ocean temperatures are at their lowest. From the SST curve, we see that the minimum temperatures occur in September, when wind stresses cause the upwelling along the coast to increase. Simultaneously, the largest quantities of carbon dioxide are released. The EOF time series shows a maximum atmospheric CO_2 concentration about a month after this occurs. This one month lag is the time that it would take for the CO_2 to be released and build up in the air above the ocean. Once the atmospheric CO_2 has reached its maximum, it is mixed rather slowly towards higher latitudes. This process takes some time, so when we see the SST reaching its highest temperatures, the atmospheric CO_2 continues to decrease. CO_2 continues to be dispersed for three to four months after the SST has peaked. It doesn't begin increasing again until the temperatures have gone back down, and stronger upwelling again starts pumping greater quantities of carbon dioxide back into the atmosphere.

The third eigenvector shows that the tropics are subject to the greatest variability from this upwelling of cold, CO_2-rich water. The fact that the whole tropical strip from 10°S to about 30°N is influenced by this upwelling shows what a strong effect this phenomenon has. It would appear to completely dominate any other activity in this region.

The third EOF no longer shows any kind of discernable pattern for the separate hemisphere analyses, either in its time series or eigenvector map. In both hemispheres, the third EOF contributes less than one percent of the variance, so it isn't surprising that the time series are chaotic and appear to be in the noise level.

4.2 Non-seasonal EOF

As with the seasonal analyses, there was one global run done with all 17 stations, using the procedure described for the non-seasonal analysis. This was followed by one run for each hemisphere. Again, the global trends can be examined and the contribution from each hemisphere can be analyzed and compared separately. Figure B-14 shows the time series for the non-seasonal EOFs. Their corresponding eigenvector maps are pictured in Figures B-15, B-16, and B-17. The hemispheric time series are given in Figures B-18 and B-19. Again, the eigenvector maps for the separate hemispheres are not included, since there are too few stations to draw any reliable conclusions. The percentages for each component are shown in Table A.2.

The first non-seasonal EOF accounts for about 97 percent of the total non-seasonal variance. Its time series shows an overall increase of almost 11.7 from 1981 to 1990. Though this upward trend seems to be very uniform from year to year, there is one feature of this graph that is a bit unsettling. Every year, in the month of January, there is a rather large step up from the previous year. Though at first it was thought to be a problem in the program, it is now believed to be a result of the following:

The mean for each month of the year is determined by averaging all ten monthly values for that particular month. Then the anomalies are determined by subtracting that mean from the original reading for that month. The most likely interpretation for what is happening is that the overall increase is large enough so that each year, the anomaly increases by a significant step. Since the seasonal variation has been taken out, the curve for each year is virtually flat, showing little or no slope for that year. However, when the next year, or in other words the next January, is encountered, there is a significant increase in the value of the anomaly. This increase is carried

throughout the year, as the other months all show a similar step up from the previous year's value. This will happen each year, creating a series of steps in the non-seasonal trend.

The first non-seasonal eigenvector shows a fairly constant distribution of the variance across the globe. From this, it can be deduced that the long term non-seasonal increase is distributed uniformly around the earth. However, the analyses for the separate hemispheres indicate that the Northern Hemisphere has a greater long term contribution than the Southern Hemisphere. This makes sense since most fossil fuel combustion occurs in the Northern Hemisphere.

The time series of the second and third non-seasonal eigenvectors, though shown with the others, have no discernable patterns and follow no known trends. The curves are chaotic and could not be related to any known surface or atmospheric features. SST, volcanic eruptions, and the El Niño were all considered, but no conclusions could be made. The percent contribution for each is less than one.

The northern and southern non-seasonal analyses showed results similar to those of the global runs. The first Northern Hemisphere EOF accounts for 96.4 percent of the total non-seasonal variance, while the first southern EOF is responsible for 98.7 percent of that hemisphere's non-seasonal variance. Both show the same step function in the transition from one year to the next for the first EOF. The Northern Hemisphere EOF shows an overall increase of almost 10 units during the ten year period, while the southern EOF shows an increase of 6.5 for the same time frame. This follows since most of the carbon being added is a result of fossil fuel combustion in the NH, so the Southern Hemisphere will not show as great an increase in the long term trend.

As with the global EOF analysis, the second and third eigenvectors do not seem to match any known patterns or events and seem to be inconclusive. They all account for less than one percent each, indicating that their role in the overall non-seasonal trend is virtually non-existent.

Chapter 5

A Second Analysis

Attention was given in Section 4.2 to the possibility that the technique used for calculating the anomaly matrices may not be satisfactory. The fact that the non-seasonal trend went up in steps instead of with a smooth slope led to question whether the anomaly matrix was continuous. Upon looking at the anomaly curves for the individual stations, it appeared that many of them increased with this step behavior. Pulling out the seasonal variation with the method described in Chapter 3 left this series of jumps, simply by the way the averages and anomalies are defined.[1] So it is inherent in the calculations that the overall trend increases in steps from one year to the next.

The possible contamination of the seasonal variation was contemplated as well. The seasonal variation shows a long-term increase, which ideally would be taken out by the calculations of the original anomaly matrix.[2] Also, it is expected that the eigenvectors for the first seasonal EOF would be of opposite sign since the two hemispheres are out of phase, but in fact, the whole map is positive. The anthropogenic contribution to that first EOF may be responsible for the lack of sign change, but the presence of the seasonal cycle with such a strong correlation to the Northern Hemisphere indicates that the hemispheres should be out of phase, and this should be reflected in the eigenvectors.

[1] See the explanation for these discontinuous steps in Section 4.2.
[2] See Section 3.2.

For these reasons, the original anomaly matrices were re-calculated using a different method of eliminating the seasonal and non-seasonal trends. This chapter outlines the differences in the procedure and the results that were obtained by this method.

5.1 Procedure

The only difference from the original procedure is the way that the anomaly matrices were calculated. A best-fit curve was determined to approximate the data at each station. A linear curve-fit was used, since there was no significant increase in accuracy by non-linear approximations. Next, the difference between the curve and the raw data was calculated. This gives a new set of values for each station, adjusted for the long term trend. From this point, the matrices can be calculated for the seasonal and non-seasonal anomalies, using the same methods described in Chapter 3. This matrix is simply substituted in place of the raw data. The rest of the EOF analysis is the same as well.

5.2 Results and Discussion

5.2.1 Seasonal EOF

Again, for the seasonal analysis, three runs were performed: one with all seventeen stations, and one for each hemisphere. The time series for the first three seasonal EOFs are shown in Figure B-20, while Figures B-21, B-22, and B-23 are their eigenvectors. The Northern Hemisphere and Southern Hemisphere EOFs are shown in Figures B-24 and B-25; again their eigenvectors are omitted. The percent contributions for each are tabulated in Table A.3.

First Seasonal EOF

The first seasonal EOF represents about 65.8 percent of the total variance. This is much lower than the variation determined by the other method. It appears that in this analysis, the first seasonal EOF reflects the changes in the land biosphere. CO_2

reaches a maximum in the spring, in April or May, and decreases throughout the summer months as plants consume it from the atmosphere for photosynthesis. The concentration reaches a minimum in the fall, about August or September, when the biosphere is on the decline. Like before, the curve drops off sharply as CO_2 is used up by plants in the spring and summer, but the increase during the winter months is more gradual, since it takes time for CO_2 to build up again through respiration.

The seasonal variance for the land biosphere is approximately 10, whereas for the earlier analysis, the amplitude was only 4. More than 65 percent of the variation is attributed to the effect of vegetation and possibly some contribution from anthropogenic cycles. As in the earlier analysis, these factors make up the largest component.

The Northern Hemisphere again dominates the Southern Hemisphere, which is evidenced by the fact that the cycle maximizes in the NH spring, and minimizes in the autumn. The time series of the Northern Hemisphere's first seasonal EOF, Figure B-24, almost identically matches the global EOF, in both shape and magnitude. The Southern Hemisphere is out of phase, which is expected since its seasonal cycle is opposite that of the Northern Hemisphere. The SH variance is not as distinguishable as that of the NH, nor is it as large; it's seasonal cycle never exceeds 6, and is inconsistent from one year to the next. These are probably due to the fact that the SH biosphere is not as extensive, and therefore will not exhibit as much seasonal variance. It is also important to note that interhemispheric transport will act to bring some of the anthropogenic CO_2 into the Southern Hemisphere, thus altering the pure signal.

The first seasonal eigenvector map has negative values for those locations in the Southern Hemisphere, and positive for the Northern Hemisphere. This indicates that the hemispheres are out of phase. That is, as the NH is taking CO_2 out of the atmosphere, it is building up in the SH. It appears that the eigenvectors increase with latitude, particularly in the Northern Hemsisphere. This would ensue from the fact that there is greater seasonal variation at higher latitudes, because the land biosphere is practically non-existent during the winter but flourishing during the

summer months. At lower latitudes there is relatively constant plant activity year round. Thus this eigenvector map, as well as the time series, exhibits the same patterns as that for the terrestrial biosphere in the previous analysis.

Second Seasonal EOF

The second seasonal EOF is not as obvious as the first. It does not appear to have a seasonal cycle, but looks chaotic. This may in fact be the residual of the difference between the line-fit approximation and the actual data. Looking at the eigenvector map may provide some insight as to where the variation is coming from. The largest values appear to be centered in the Southern Hemisphere somewhere between 20°S and 60°S. Smallest values are at approximately 60°N. If the best-fit line used to determine our anomaly matrix physically approximates the average amount of anthropogenic carbon being added to the atmosphere over time, then this second eigenvector may represent the deviation from that value. For instance, it is known that most carbon being added by fossil fuel combustion is being injected in the Northern Hemisphere between 20° and 60° latitude. So, at any time, the deviation from the anthropogenic input will be very small in this region, since it is close to the source. However, it takes about 320 days [13] for CO_2 to be distributed globally. So, the variation near the South Pole will be largest, since it will take longest for changes in carbon injection to reach that distance. The map reflects all of these characteristics.

If it weren't for the spacial maps created by the eigenvectors, it would be difficult to differentiate this from the El Niño signal, which is discussed in Section 5.2.2. However, because of the distribution of the variance, it is clear that this cannot be the El Niño, which would affect the tropical strip, not the higher latitudes.

The results for the Northern and Southern Hemisphere do not appear to be chaotic. In fact, the time series for the Northern Hemisphere has a cycle almost identical to that of the third seasonal EOF.[3] The Southern Hemisphere seems to be of approximately the same phase as the Northern Hemisphere, but its signal is not as clear. The amplitudes for both hemispheres are of similar magnitudes; always less

[3]This cycle will be discussed in the next subsection.

than 4, but highly variable. So it would appear that the variations indicated by the second hemisphere-specific EOFs match the third global EOF.

Third Seasonal EOF

The third EOF shows a very clear seasonal cycle. It reaches a maximum in November or December, and a minimum in June or July. This pattern is quite similar to that of the third EOF for the first analysis. It's amplitude is between 3 and 4 here, but in the earlier graph, it was only 2. This component now accounts for almost 7 percent of the variance, whereas before it was only responsible for one percent. So the question becomes, is this component also evidence of the high CO_2 upwelling and its effect on tropical strip?

The eigenvector map may help to answer this question. The tropical strip again appears to be of opposite sign to the rest of the world. All the values in this region are negative. There is one station in the Southern Hemisphere that is also negative, but it is an extremely small negative number, and could therefore be attributed to error. Also, its location is off the tip of South America, so it could be feeling the effects of the upwelling in the tropics being carried southwards.

The third EOF accounts for about 6.8 percent of the total variance. It has a seasonal amplitude of about 4 units, which is less than half the amount contributed by the first EOF. This implies that the terrestrial biosphere contributes much more to the seasonal variance than this upwelling component does. So, the magnitude of the seasonal breathing of CO_2 by the land biosphere is more than twice as great.

The third EOFs for the separate hemispheres show no discernable seasonal variations. Both have magnitudes of less than three, and are responsible for less than eight percent of the total variation. They would appear to be down in the noise level of the analysis.

5.2.2 Non-Seasonal EOF

As before, three runs were made. One was for the global analysis with all 17 stations. The next was for the 12 Northern Hemisphere stations, and finally the 5 in the

Southern Hemisphere. Time series for the first three EOFs are shown in Figure B-26, and it's associated eigenvectors are seen in Figures B-27, B-28, and B-29. The Northern and Southern Hemispheric runs are pictured in Figures B-30, and B-31, and again, only their time series are shown.

The first non-seasonal EOF describes about 52 percent of the total trend. It has a range of about ten for the entire time period. There are two periods of extremely low atmospheric carbon dioxide concentration. These coincide with the activity of the El Niño! Figure B-32 shows the occurrences of the El Niño for the relevant time period [4]. In late 1982-1983, there was a very strong El Niño. The first non-seasonal EOF shows a sharp decrease in the amount of atmospheric CO_2 at this time. In 1986-1987 another El Niño occurred, though this time not as strong as before. Simultaneously, the EOF time series shows another dip, somewhat smaller than the first. The analyses for the two separate hemispheres show extremely similar curves. The same highs and lows appear in each. The pattern in the Southern Hemisphere is a bit more marked, further indicating that it may well be the El Niño, since the signal would be strongest in that hemisphere, where it originates. It therefore seems that the El Niño is directly tied to the concentration of atmospheric carbon dioxide [14].

Most of the time, there is a strong upwelling in the Eastern Pacific Ocean. This upwelling brings up colder water that is rich in nutrients as well as CO_2. During the phenomenon known as the El Niño, this upwelling decreases drastically. The water is warmer, and contains fewer nutrients. The question relative to CO_2 has been, when is this region contributing to atmospheric CO_2 content, and when is it decreasing it? While the upwelling is present, the water is rich in CO_2. So excess carbon dioxide will be added to the atmosphere. However, there are also more nutrients in the water, allowing for more photosynthesis to occur, which would actually take more CO_2 out of the air. When the El Niño occurs, the opposite effect will be created. Therefore, the argument can go either way as to whether the El Niño encourages CO_2 uptake by the ocean, or increases its injection into the atmosphere.

From the time series of the first non-seasonal EOF and the El Niño, it seems clear that the presence of the El Niño acts to diminish the source of carbon dioxide to the

atmosphere. This means that when the upwelling occurs, CO_2 is being added to the atmosphere. So according to this analysis, the effect of the excess CO_2 outweighs that of the enhanced nutrient supply in the upwelling water!

The associated eigenvector map partially supports this theory. The two stations in the middle Pacific have higher values than the rest of the globe. There are also greater values with increasing latitude in the Southern Hemisphere. This is probably due to the fact that since the El Niño emanates from the Southern Hemisphere, it will be felt the strongest in this hemisphere. Also, since the effect of the upwelling in this region has already been discussed, it makes sense that the two stations in the tropical Pacific will show a great variability in response to this effect. Indeed, we see this reflected in the eigenvectors. Unfortunately, there are no stations in the Eastern Pacific near the South American coast to make this hypothesis concrete. If data were collected at the Cosmos/Huancayo station in Peru, this theory could either be decidedly verified or dismissed[4].

The time series for the individual hemisphere analyses show a similar curve for the first EOF. The magnitudes and variations in both curves are extremely similar to that of the global example.

It was questioned as to whether this EOF really was following the trend of the El Niño, or if it was actually similar to the second EOF of the seasonal analysis, and was a reflection of the anthropogenic input. Both graphs seem to be quite similar. However, it does not seem likely that it is the anthropogenic input, because the weighting of the eigenvectors would not fit with that theory.

The other EOF time series for the non-seasonal case appear to be lost in the noise level of this analysis. There is no noticeable trend in any of these other graphs, for either the global or hemisphere-specific cases.

[4]Data was collected sporadically at Cosmos/Huancayo for 1984 and 1985 [17].

Chapter 6

The Missing Sink

There have been numerous explanations offered for the 'missing sink' of carbon dioxide. Many different models have been expounded revolving around atmosphere-ocean interaction, only to be discredited by later models. The following chapter is a brief look at some of the more recent ideas in the search for the carbon dioxide sink.

Prior to 1990, it was popularly believed that the ocean was somehow responsible for the disappearance of the excess CO_2. Box diffusion models used Carbon-14 added to the air by nuclear testing in the 1950s as a tracer for carbon transport in the ocean. Such models predicted an oceanic uptake of approximately 2 Gigatons of carbon per year. Three dimensional ocean circulation models predicted similar values [27]. Then in 1990, a paper by Pieter Tans and associates presented a new theory [23]. It claimed that Carbon-14 and other tracers were not an accurate measure of carbon dioxide in the ocean. Instead, the partial pressures of CO_2 in the ocean surface waters and the concentrations of atmospheric CO_2 were used in the model calculations. The difference δpCO_2 represents the potential for CO_2 to move across the air-sea boundary. Using this premise, it was determined that there were limits on the amount of CO_2 the northern oceans could absorb. It was also decided, upon examination of the meridional gradient, that atmospheric transport of CO_2 from the Northern Hemisphere to the Southern Hemisphere is limited. The final result was that the ocean is only responsible for taking up 0.3-0.8 Gt of carbon per year, leaving between 1.5 and 2.0 Gt unaccounted for. A hypothesis was made that there must be

a terrestrial sink at temperate latitudes to properly balance the north-south gradient of atmospheric CO_2. Before this time, a large terrestrial sink hadn't really been considered in much detail.

In 1992, Broecker and Peng published a paper showing that the CO_2 sink might not necessarily have to be some large value attributed to high latitude forests, but may in fact be accounted for by a natural north to south transport of CO_2 dissolved in the oceans [3]. This is due to the greater PO_4 content of Antarctic waters, which leads to enhanced levels of respiration CO_2. Therefore, the surface waters in the Northern Hemisphere are able to absorb more atmospheric CO_2 than those of the Southern Hemisphere, thus setting up a north to south oceanic pump. This is countered by a south to north atmospheric transport. However, since the Industrial Revolution, these motions have reversed. The greater concentration of atmospheric CO_2 in the Northern Hemisphere has caused the atmospheric motion to carry CO_2 from north to south, in turn forcing the ocean pump to go the opposite direction. Broecker and Peng argue that the northern mid-latitude terrestrial sink need not be as large as Tans had projected, since the normal tendency for north to south oceanic transport reduces the gradient, but that a smaller land-based sink may still be necessary to balance the CO_2 budget.

Simultaneously, a paper was published by Sarmiento and Sundquist [20] challenging some of the assumptions Tans' paper made. They pointed out the skin-temperature effect, that is that surface water temperature is usually a bit colder than that of the rest of the ocean. It was estimated that this would increase the CO_2 flux into the ocean by 0.14-0.54 Gt of carbon per year. Another effect that they discuss is the oxidation of carbon monoxide given off by the combustion of fossil fuels, to carbon dioxide. It is thought that this contribution actually accounts for the loss of 0.25-0.29 Gt of carbon per year from the Northern to Southern Hemisphere. Yet another factor that they consider significant is the flux of CO_2 into the ocean by rivers and streams. Their conclusion is that if all of these are considered, then Tans' calculations will be in much closer agreement with the general circulation models. Sarmiento and Sundquist agree that there will still be a need for a terrestrial sink,

but that it will be of much smaller magnitude than Tans originally claimed.

Since then, there have been arguments for the presence of a northern mid-latitude terrestrial sink, as well as arguments against it. Some studies have been done on land where logging has been conducted. However, they only took into account the consumption of atmospheric CO_2 by regrowth, and not its addition by the decay of dead plantlife. Another analysis examined how climate change and CO_2 have interacted in recent years by looking at net primary production and soil respiration in response to temperature and rainfall. It concluded that there could indeed be a carbon sink of almost 25 Gigatons from 1950-1984. Yet another study utilizing forest surveys declares that there is no way that the northern mid-latitudes could provide such a sink [24].

Unfortunately, all of these models are but approximations and simplifications of atmospheric, oceanic, and terrestrial processes. No one can say for sure which models are right, or even which assumptions are the best. For so long many agreed that the oceans were the missing sink, but now attention has turned to the northern temperate land regions. Even with all of these different studies and analyses, the basic question of where the missing sink lies is still unanswered.

Chapter 7

Conclusion

7.1 Summary of Results

Though this study was broken into two parts, it would seem that many of the conclusions from both techniques actually fit together quite well. For easier discussion, the first set of runs will be referred to as T1, and the second set, using the best-fit curve, will be T2.

The non-seasonal trend for T1 emphasizes the fact that the concentration of CO_2 is steadily increasing with time. It also makes clear the fact that atmospheric CO_2 content is growing smoothly, with no jumps or skips in the record, but simply a steady increase.

The first eigenvector of T1 sets up an excellent time series outlining the overall effect of the various factors in the atmospheric carbon dioxide cycle. It's largest components are believed to be the seasonal breathing of the land biosphere, and the long-term trend of the anthropogenic carbon input to the atmosphere. Other components may be included as well, but they are hidden beneath these larger signals.

The second seasonal EOF for T1 is very similar to the first seasonal EOF of T2. They both very clearly show the seasonal variation of the terrestrial biosphere. The maximum atmospheric CO_2 concentration is measured in April or May, and the minimum is seen in August. Therefore, the seasonal contribution of the land biosphere is completely dominated by the Northern Hemisphere. This makes sense because most

of the land mass is located there, providing a greater area for plants to grow, and thus for seasonal variation to occur. One of the most interesting results of the study was found in T1: the overall trend for the land biosphere is actually decreasing with time, while it's seasonal amplitude is actually growing. These findings support the idea that deforestation in the tropics is having a significant effect on the carbon dioxide cycle. If tropical rainforests are decreasing, then the total contribution of the land biosphere will be decreasing. Meanwhile, the seasonal variability will increase, since the more variable high-latitude forests will gain influence as the rainforests disappear. The results do indeed show both of theses features.

The third seasonal EOFs for both T1 and T2 show the contribution of the cold water upwelling off the coast of Peru, in the Eastern Pacific. It would appear that this relatively small area of upwelling dominates the entire tropical strip from about 10°S to 30°N. Despite what stresses the rest of that strip may have, the presence of upwelling is what controls the whole area. The upwelling brings up large quantities of CO_2-rich water from great depths. This CO_2 is then rapidly released into the atmosphere in that region, affecting the entire tropical strip. This result also supports the findings of the non-seasonal EOF for T2.

The first non-seasonal trend of this EOF seems to follow the pattern of the El Niño events. When the El Niño brings warmer water into the region, the concentration of atmospheric CO_2 decreases. During periods of upwelling, CO_2 concentration is significantly higher. This means that the effects of increased levels of CO_2 are winning out over the enhanced nutrient concentrations in the deep water. The nutrients would cause photosynthesis to increase, and use up atmospheric CO_2, but the excess CO_2 dissolved in the water would work to increase atmospheric CO_2 levels. So there are two forces at work in opposite directions, both due to this upwelling cold water. According to the results of both this and the third seasonal eigenvectors, the carbon dioxide effect is strongest, and the upwelling directly increases atmospheric CO_2.

The second seasonal EOF for T2 is believed to show the deviation from the average anthropogenic component that was estimated by the best-fit curve. How this exactly fits into the seasonal cycle is not understood. The smallest eigenvectors are

centered on about 60°N, and this has been attributed to the location of the source for anthropogenic CO_2. However, the largest eigenvectors are centered on 40°S. It is not known what process may be causing this distribution of the variance. It is possible that this effect may have something to do with the "Roaring 40s" of the Southern Hemisphere. This will have to be a question that is left for future studies, perhaps to be solved only once there is increased atmospheric CO_2 data available.

7.2 Recommendations for Improvement

The results of this study should be viewed with caution for several reasons. First of all, the data from the monitoring stations may not be extremely accurate. Some stations take readings daily, while others only take three or four per month. This may not lead to the best representation of data for such a station. Also, periodic calibrations are made to the raw data. Unfortunately, it often takes several years for such adjustments to be published. The data in this analysis was reviewed in an attempt to pull out any of the stations with suspicious results, but this led to the problem of having relatively few stations for a fairly short time period. The observing stations are also not evenly distributed, so more weight is given to activity in certain areas. Compromises had to be made to get a reasonable number of stations with measurements spanning a long enough time to obtain results that actually showed a trend, and still reflected something real.

Ideally, this analysis should be done with at least fifty stations scattered evenly around the globe, with continuous measurements and frequent calibrations made at each one. This way, a much more accurate history of CO_2 changes and trends could be determined. Unfortunately, it would take a lot of time, not only for such stations to be set up and manned, but until a record of significant length could be collected and studied.

7.3 Final Comments

So has the case of the missing sink been solved? It would seem that though this study might provide more clues as to the possible sources and sinks of carbon dioxide, it hasn't really answered that burning question. The long-term contribution from the land biosphere appears to be decreasing. If the theory of a large terrestrial sink in the Northern Hemisphere temperate zones is true, then its depletion could be the cause for many problems in the future. Though the contribution of the ocean, as described by the upwelling component, is not significantly changing size, it is fairly small in relation to the land biosphere. Neither the oceanic contribution nor the land biosphere component meet the expectations that we would have for them if they were a large CO_2 sink. So the carbon dioxide sink still eludes us. But the solution is out there, and with continued studies, it will hopefully be found in the near future.

Appendix A

Tables

Table A.1: Stations

STATION	LOCATION	LAT	LONG	ALT	ENVIRONMENT
Alert	NW Canada	82 31'N	62 18'W	210 m	Tundra
Amsterdam Island	Indian Ocean	37 47'S	77 31'E	65 m	Island Seashore Cliff
Amundsen-Scott	South Pole	89 59'S	24 48'W	2810 m	Snow-covered Plateau
Ascension Island	South Atlantic	07 55'S	14 25'W	54 m	Island Seashore
Cape Kumukahi	Hawaii, USA	19 31'N	154 49'W	3 m	Island Seashore
Cape Matatula	Samoa	14 15'S	170 34'W	42 m	Is Rocky Promontory
Cold Bay	Alaska, USA	55 12'N	162 43'W	11 m	Treeless Peninsula
Key Biscayne	Florida, USA	24 40'N	80 12'W	3 m	Coastal Island Seashore
Mariana Islands	Guam	13 26'N	144 47'E	2 m	Island Seashore
Mauna Loa	Hawaii, USA	19 32'N	155 35'W	3397 m	Island Tundra
Mould Bay	NW Canada	76 14'N	119 20'W	57.6 m	Island Tundra
Niwot Ridge	Colorado, USA	40 03'N	105 38'W	3749 m	Alpine Mountain
Ocean Station M	North Atlantic	66 00'N	02 00'E	6 m	Open Ocean
Palmer Station	Antarctica	64 55'S	64 00'W	33 m	Barren Island Seashore
Point Barrow	Alaska, USA	71 19'N	156 36'W	11 m	Arctic Coast
St Croix	US Virgin Islands	17 45'N	64 45'W	3 m	Island Seashore
Terceira Island	Azores	38 45'N	27 05'W	30 m	Island Seashore

Table A.2: Percent Contribution of Eigenvalues

Seasonal	Percentage	Error
EOF 1	84.9	11.0
EOF 2	11.3	1.5
EOF 3	1.5	0.2
NH Seasonal	Percentage	Error
EOF 1	91.6	11.8
EOF 2	5.5	0.7
EOF 3	0.8	0.1
SH Seasonal	Percentage	Error
EOF 1	98.3	12.7
EOF 2	0.5	.06
EOF 3	0.3	.03
Non-Seasonal	Percentage	Error
EOF 1	97.0	12.5
EOF 2	0.7	.09
EOF 3	0.5	.06
NH Non-Seasonal	Percentage	Error
EOF 1	96.4	12.4
EOF 2	0.9	0.1
EOF 3	0.6	.08
SH Non-Seasonal	Percentage	Error
EOF 1	98.7	12.7
EOF 2	0.3	.03
EOF 3	0.1	.01

Table A.3: Percent Contribution of Eigenvalues for Curve-fit EOF

Seasonal	Percentage	Error
EOF 1	65.8	8.5
EOF 2	17.3	2.23
EOF 3	6.8	0.9
NH Seasonal	Percentage	Error
EOF 1	85.2	11.0
EOF 2	8.8	1.1
EOF 3	1.5	0.2
SH Seasonal	Percentage	Error
EOF 1	65.0	8.4
EOF 2	19.0	2.5
EOF 3	7.4	1.0
Non-Seasonal	Percentage	Error
EOF 1	52.2	6.7
EOF 2	10.6	1.4
EOF 3	6.9	0.9
NH Non-Seasonal	Percentage	Error
EOF 1	50.0	6.4
EOF 2	10.9	1.4
EOF 3	8.5	1.1
SH Non-Seasonal	Percentage	Error
EOF 1	74.6	9.6
EOF 2	11.2	1.4
EOF 3	6.1	0.8

Appendix B

Figures

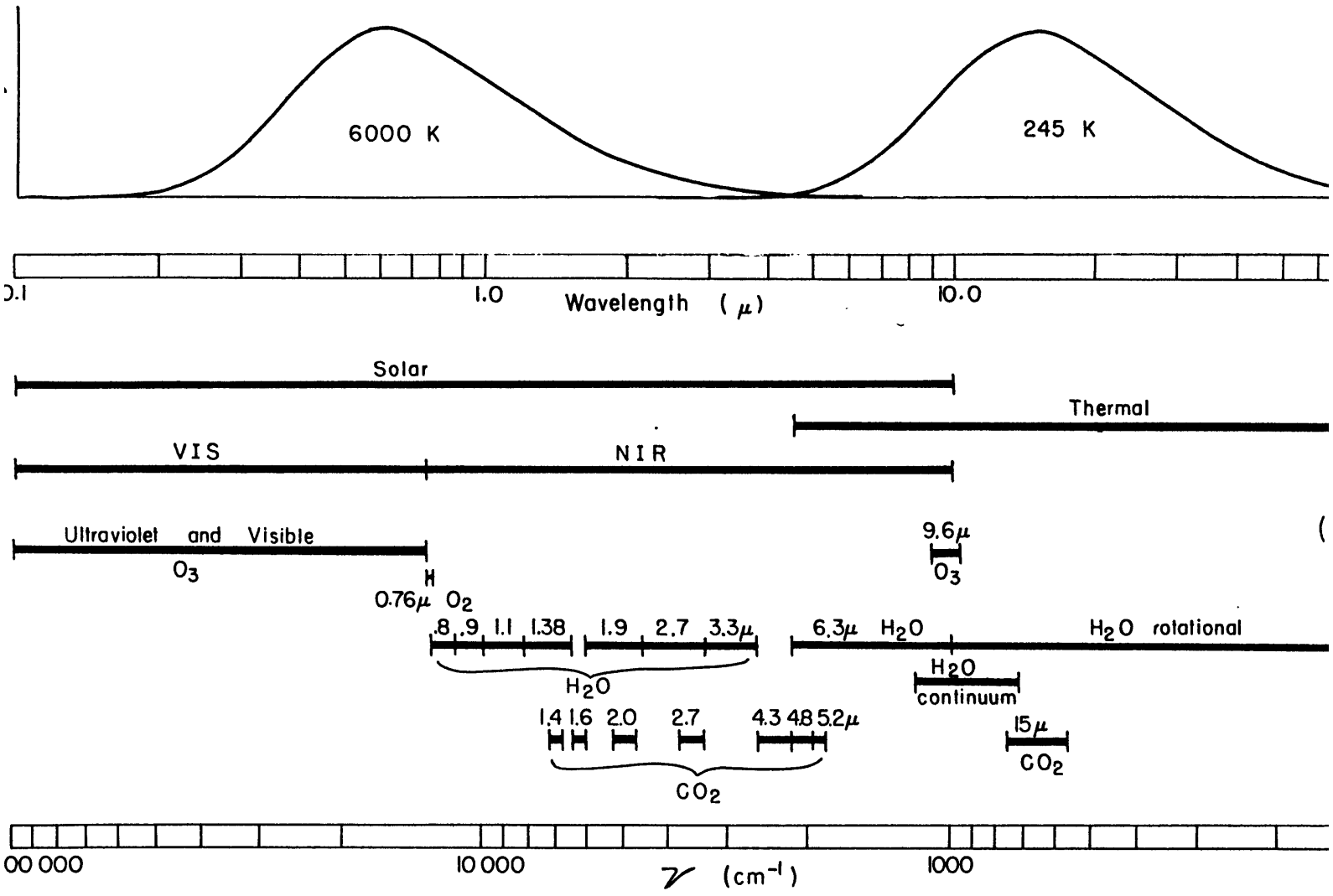

Figure B-1: Schematic description of the spectrum. The black body curves (a) after Rodgers (1974)) drawn so that the area under each curve is proportional to energy and the two curves are normali so that they enclose equal areas. The various divisions of the spectrum used in this report and absorption bands which are included in the calculations are shown in (b). [7]

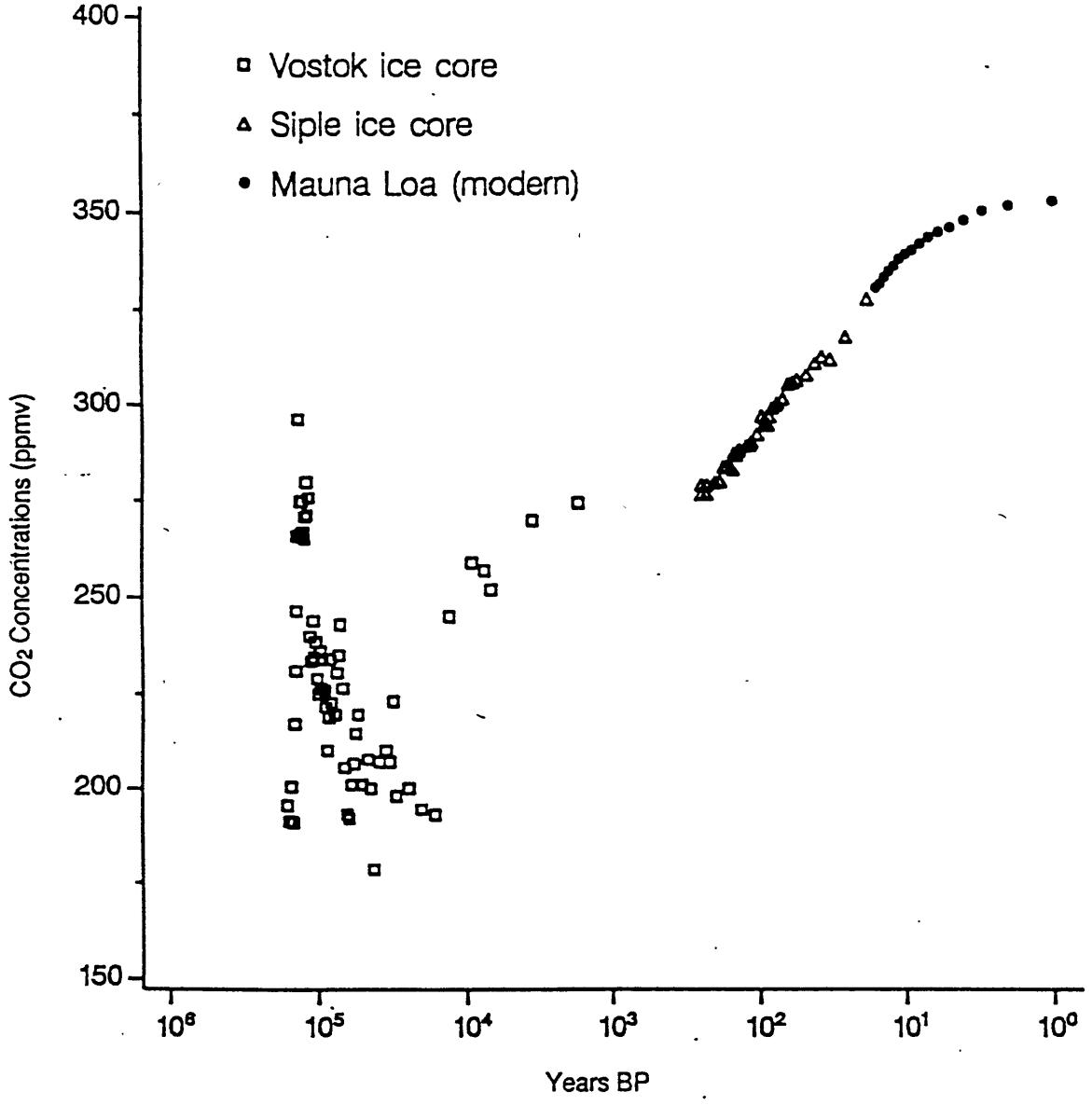

Figure B-2: Annual atmospheric CO_2 concentrations during the past 160,000 years. [25]

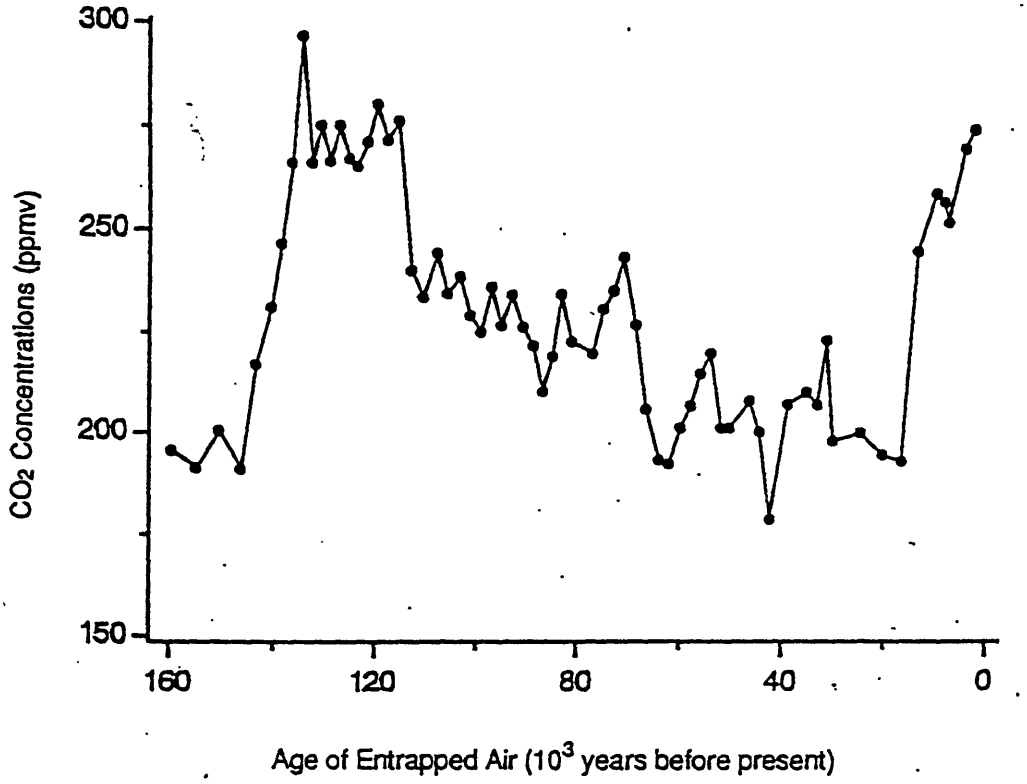

Figure B-3: Atmospheric CO_2 derived from the Vostok ice core. [25]

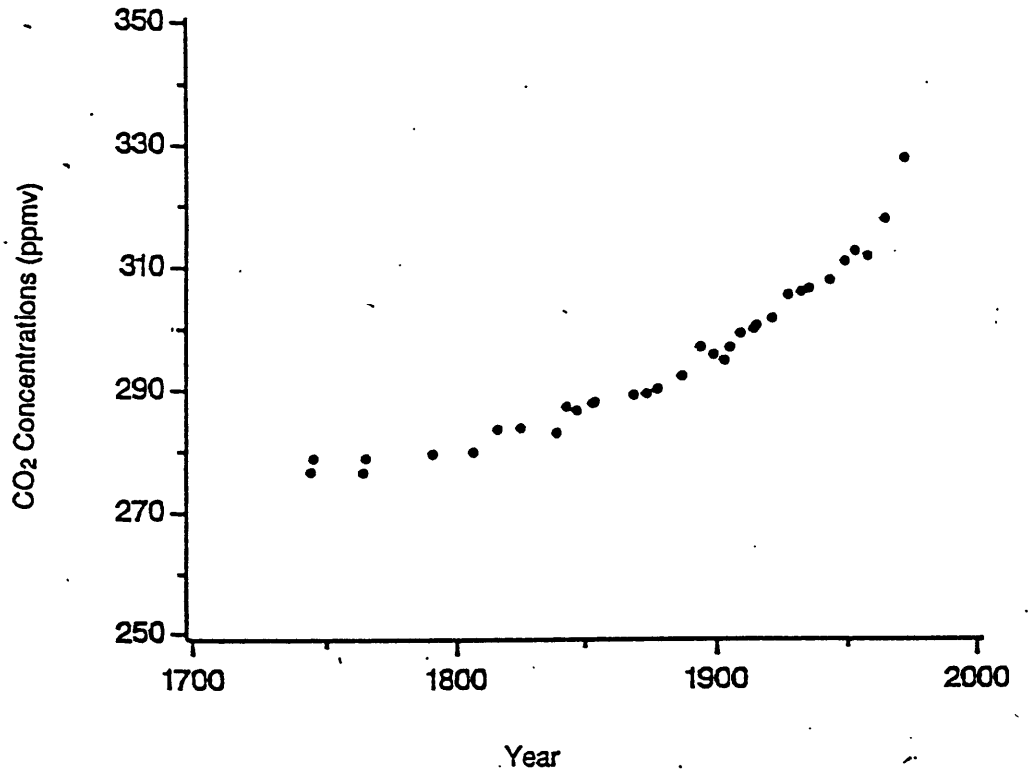

Figure B-4: Atmospheric CO_2 derived from the Siple ice core. [25]

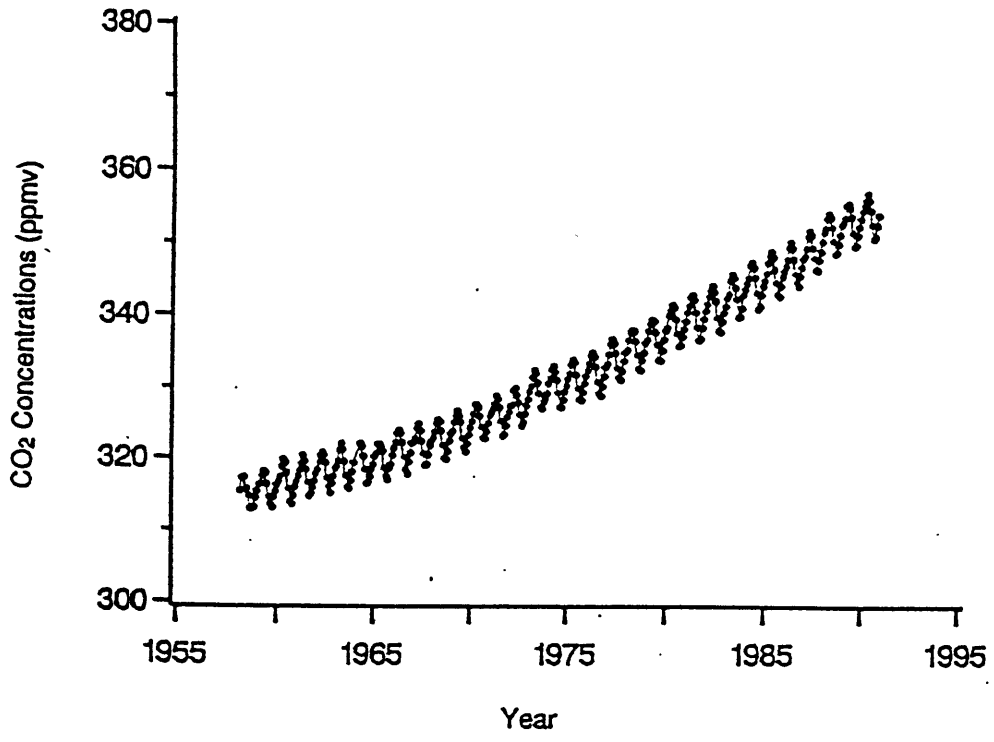

Figure B-5: Monthly atmospheric CO_2 concentrations at Mauna Loa, Hawaii. [25]

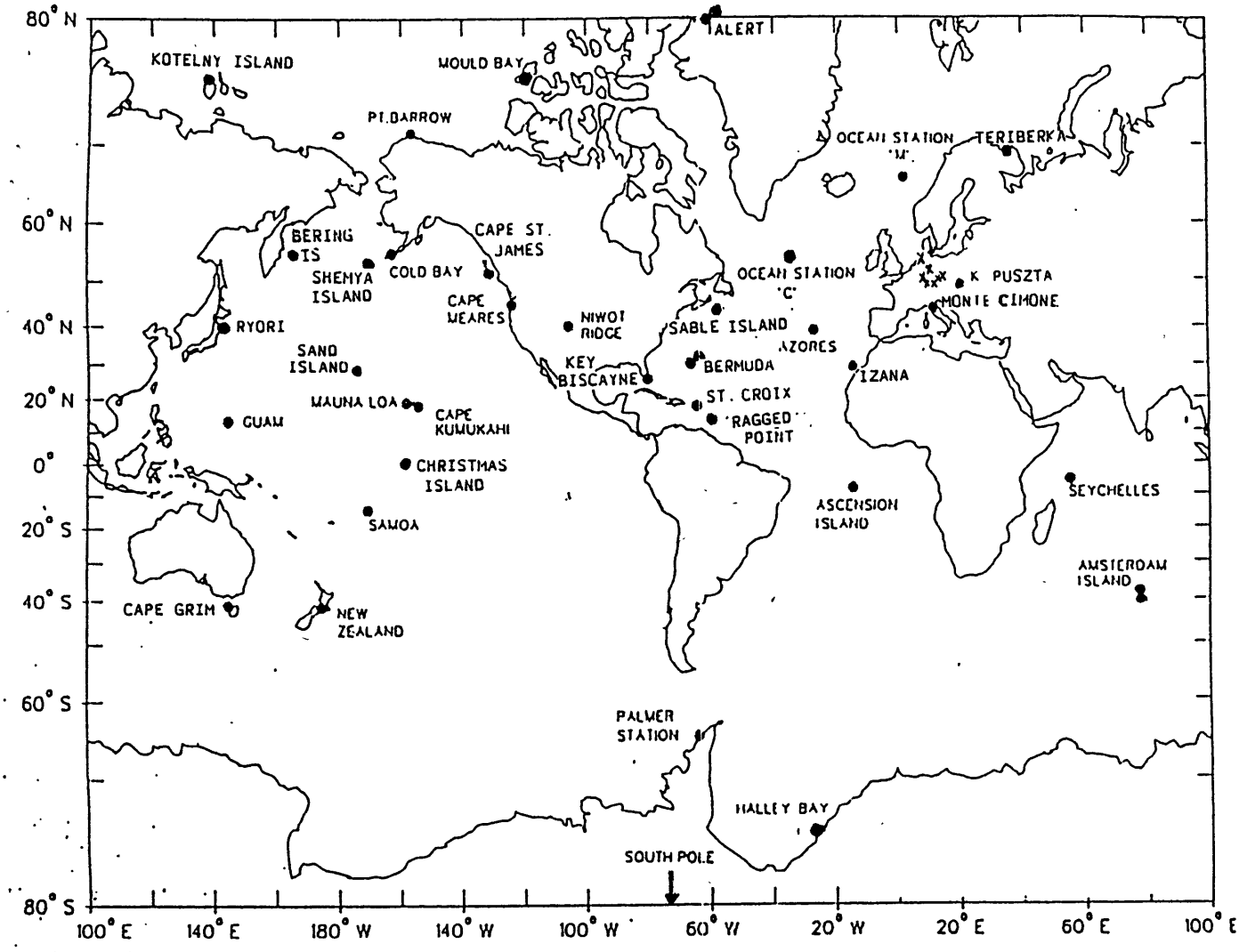

Figure B-6: Location of sites where atmospheric CO_2 is sampled.

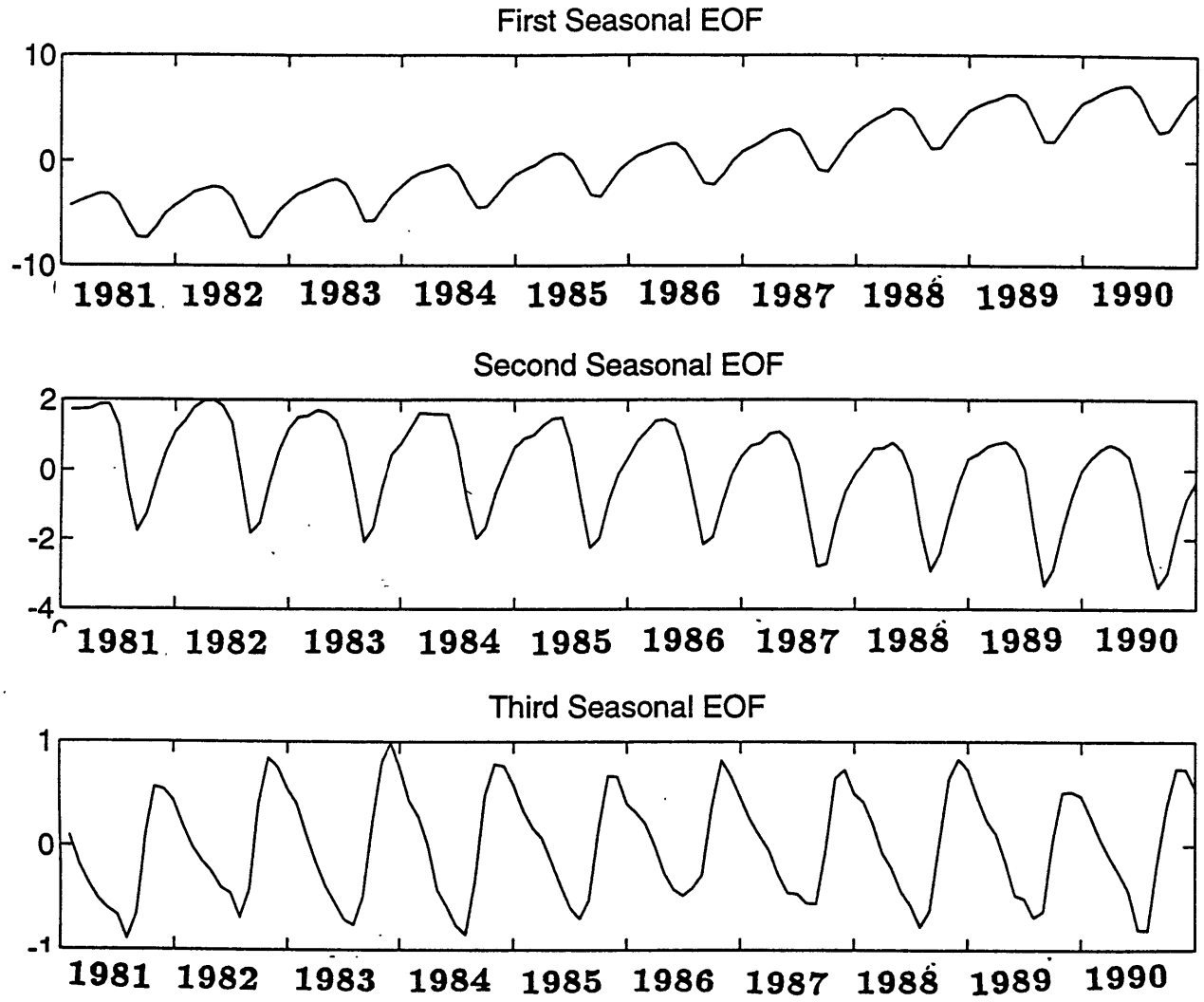

Figure B-7: Seasonal EOF

First Seasonal Eigenvector

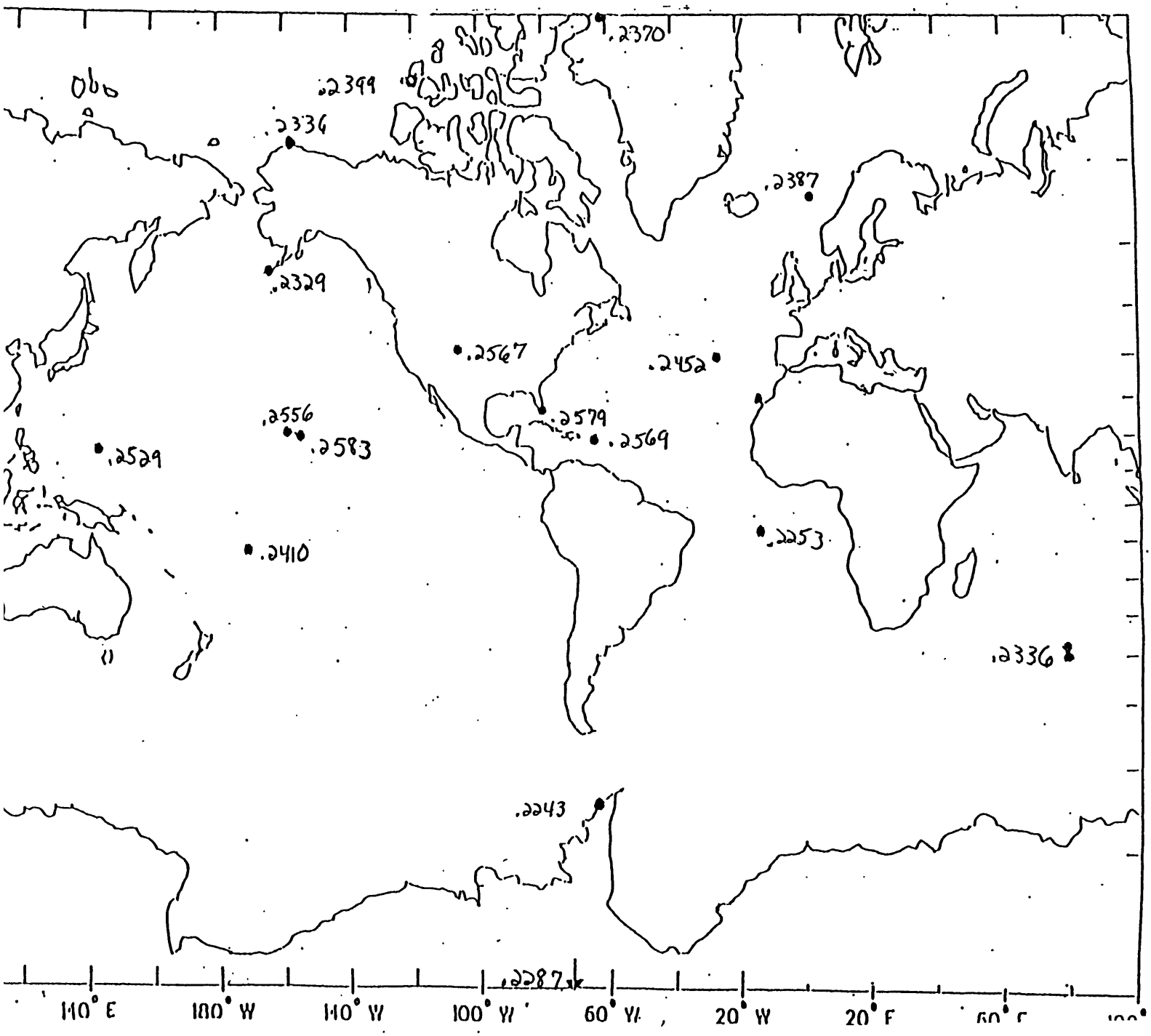

Second Seasonal Eigenvector

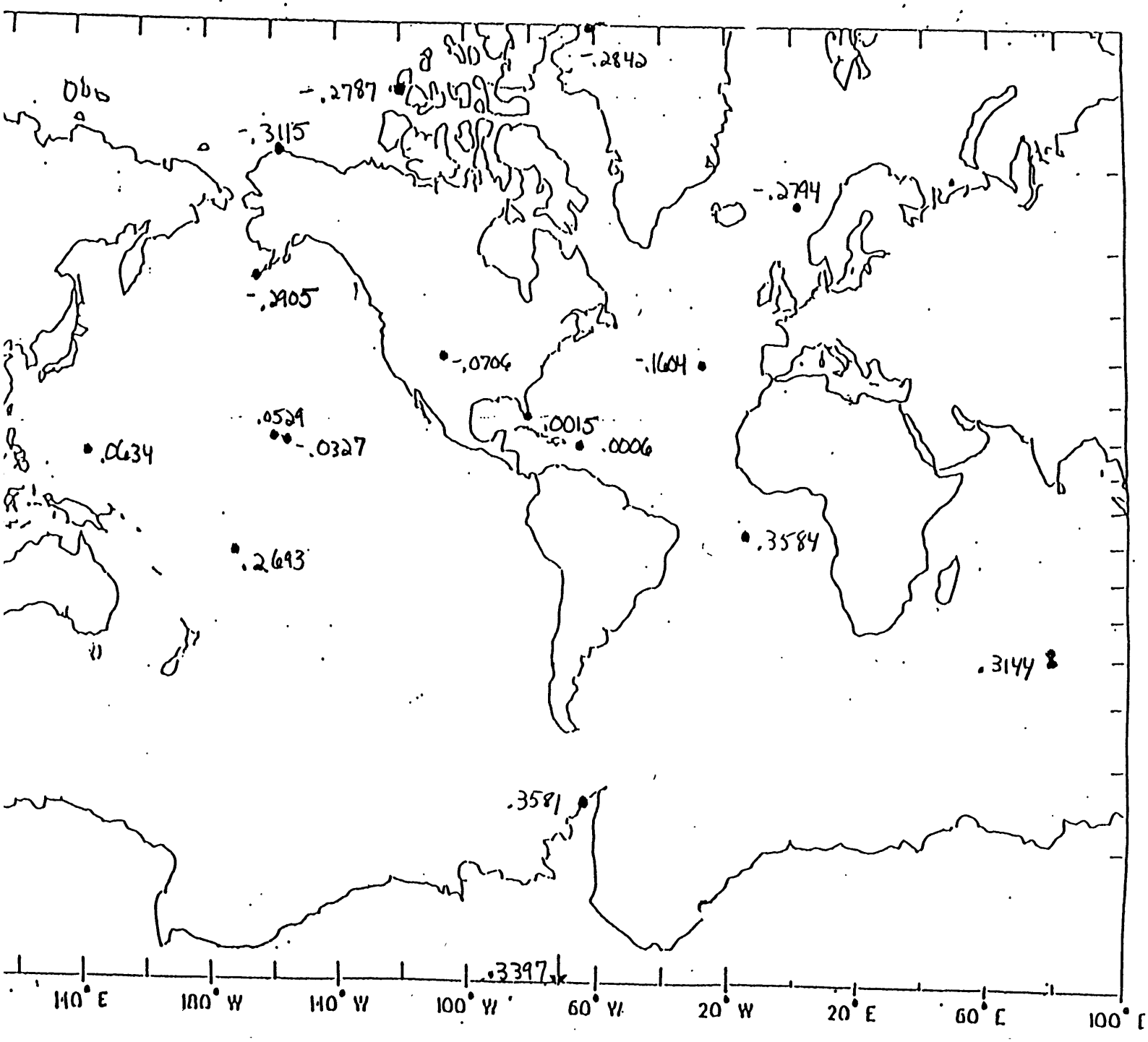

Third Seasonal Eigenvector

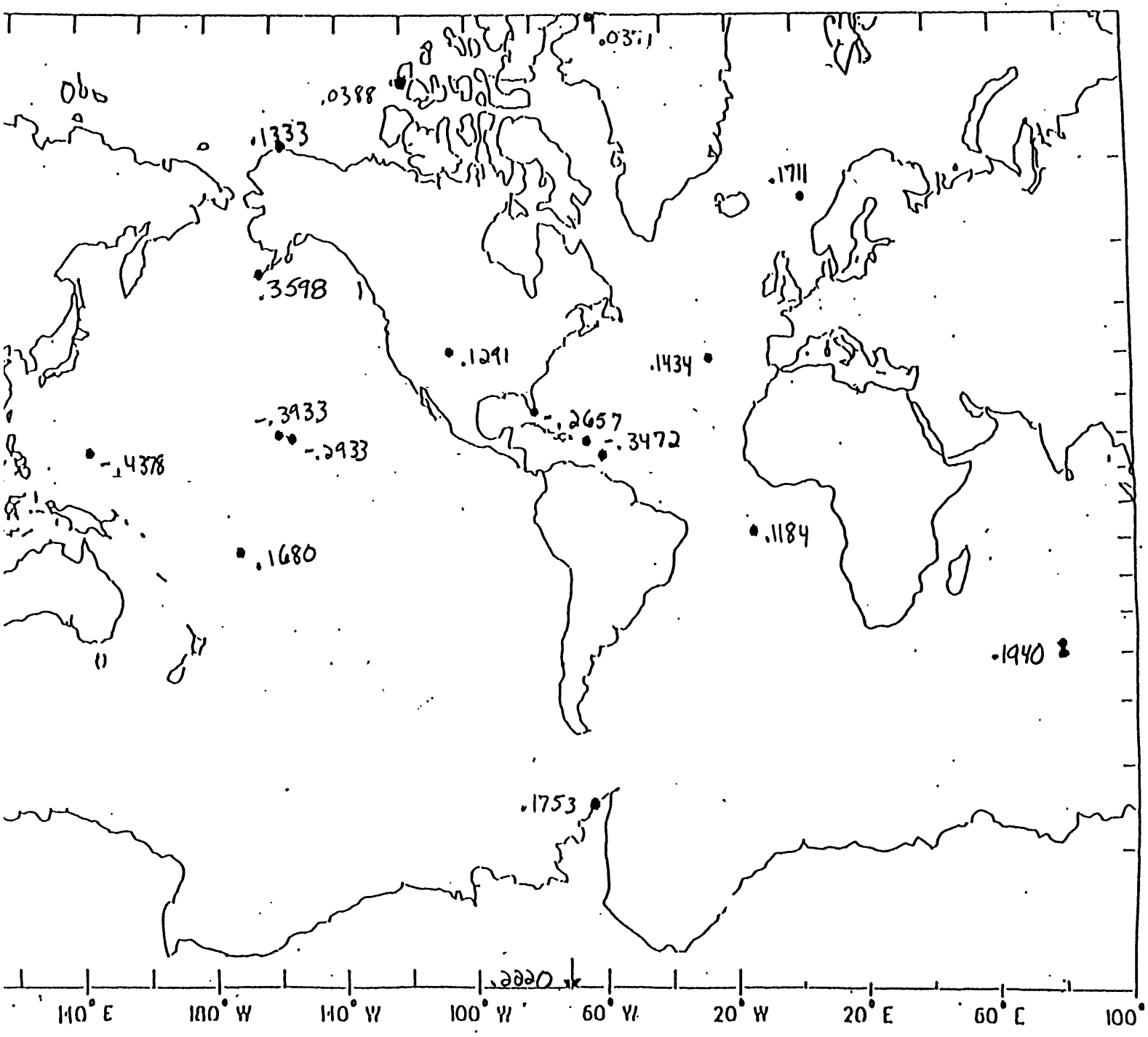

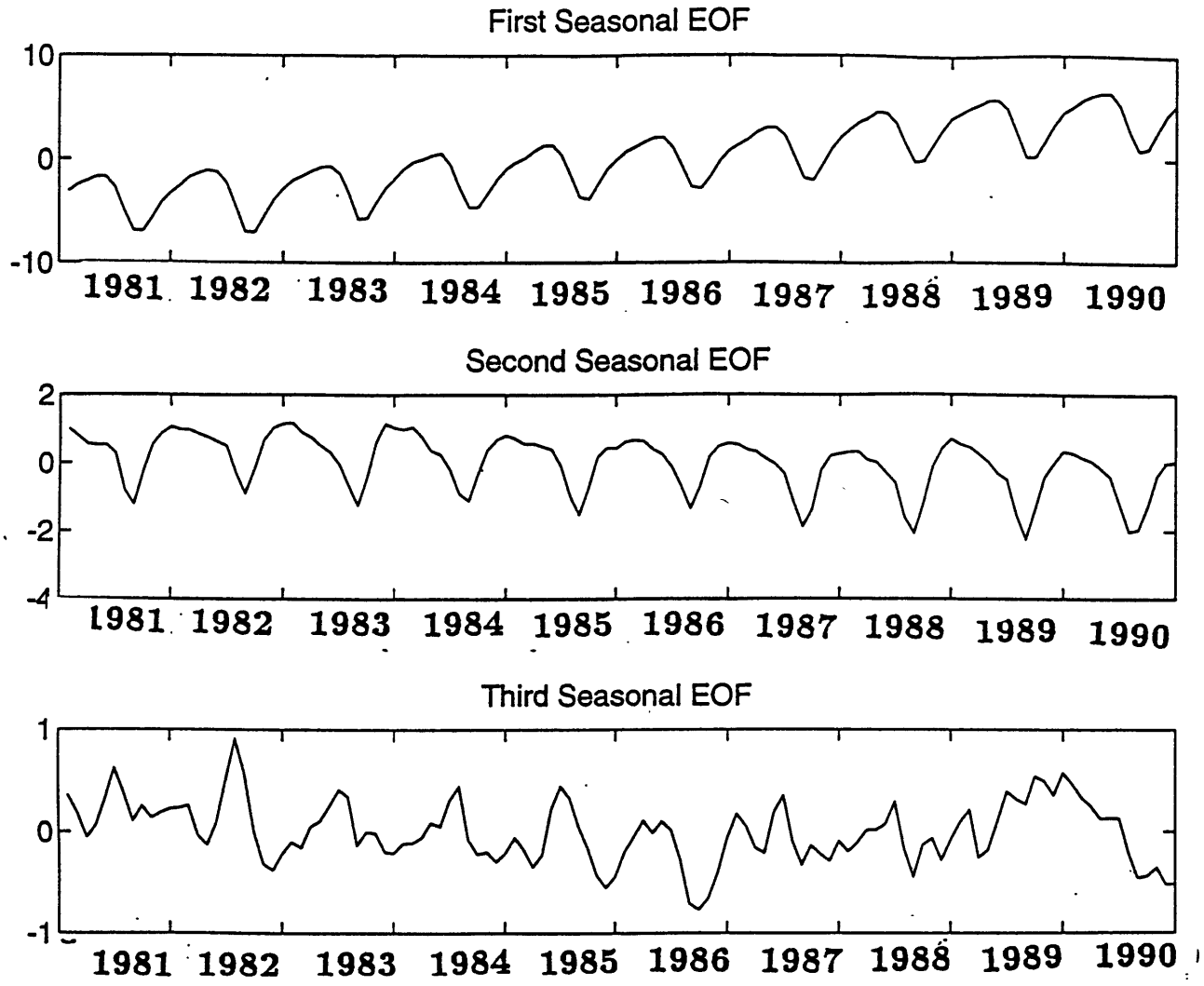

Figure B-11: Northern Hemisphere Seasonal EOF

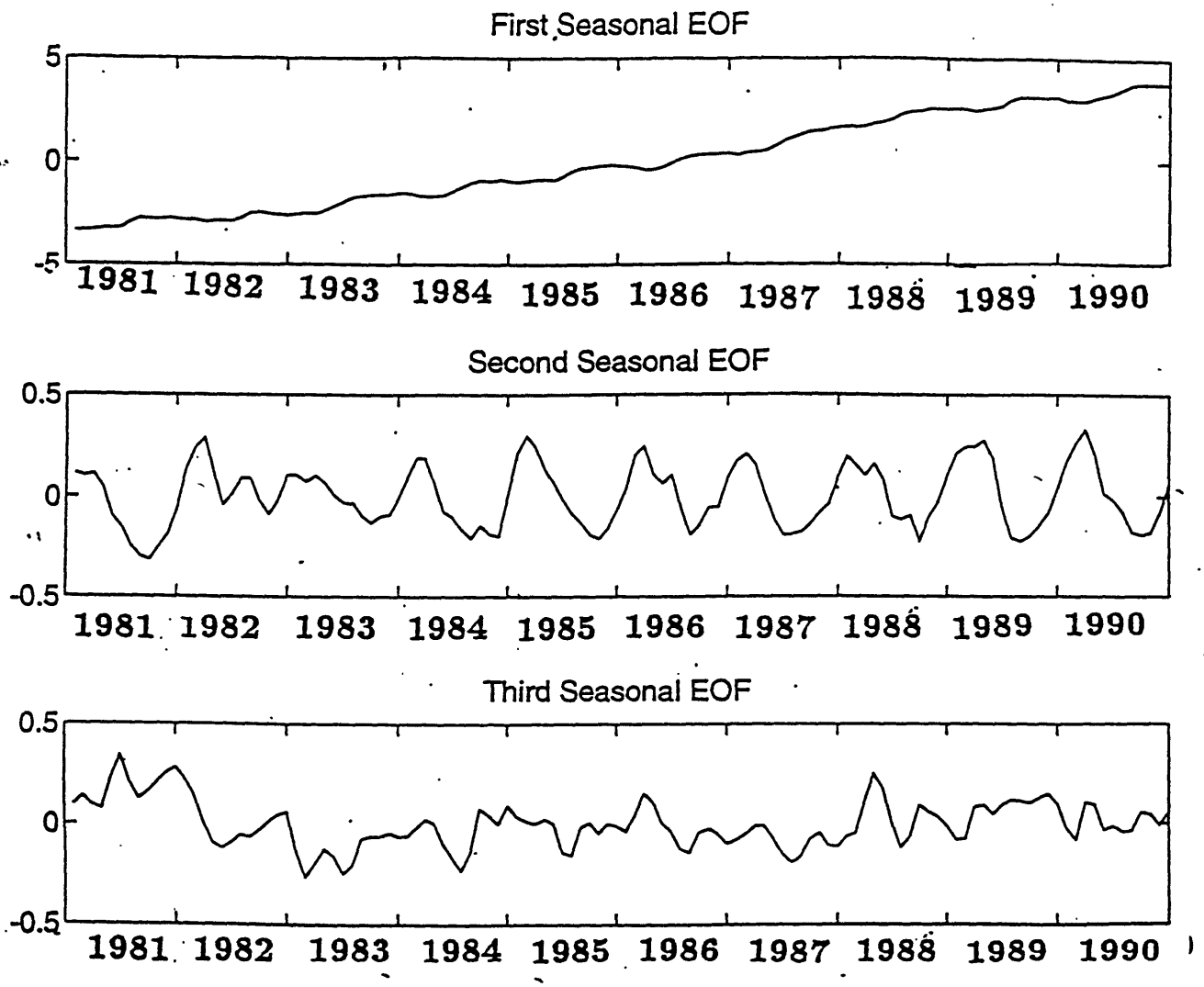

Figure B-12: Southern Hemisphere Seasonal EOF

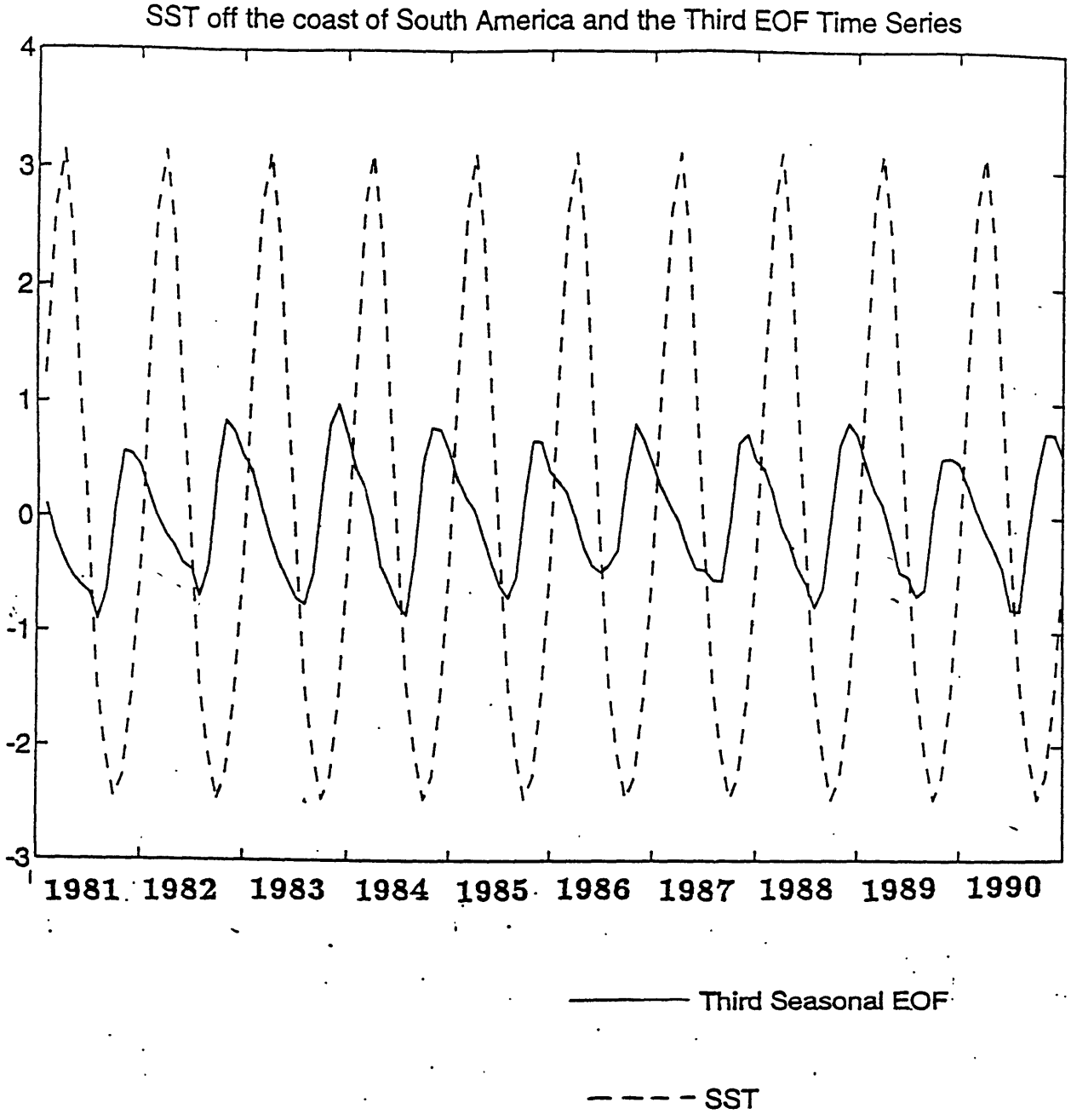

Figure B-13: Sea Surface Temperature off the west coast of South America [4] and Third Seasonal EOF

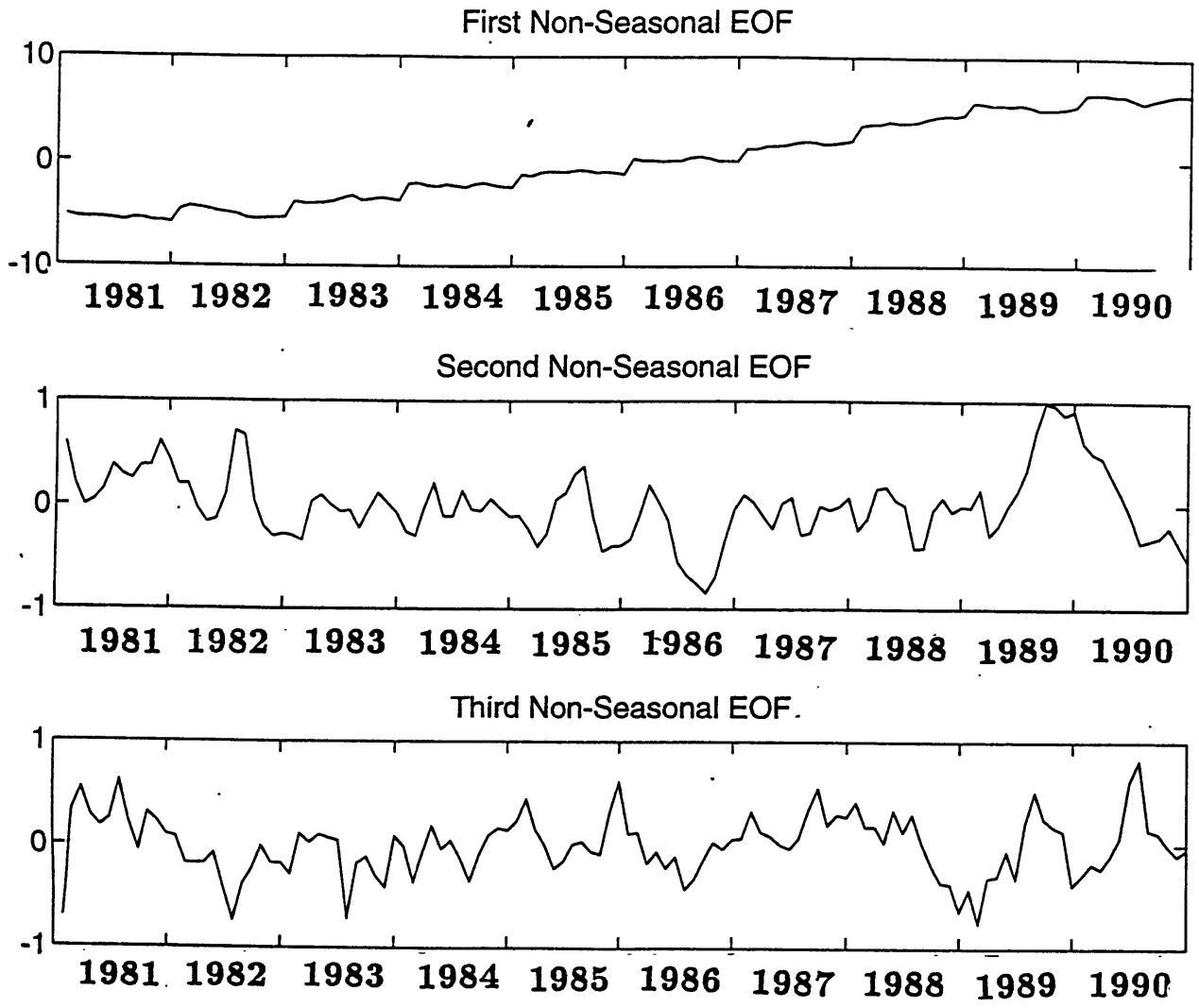

Figure B-14: Non-Seasonal EOF

First Non-Seasonal Eigenvector

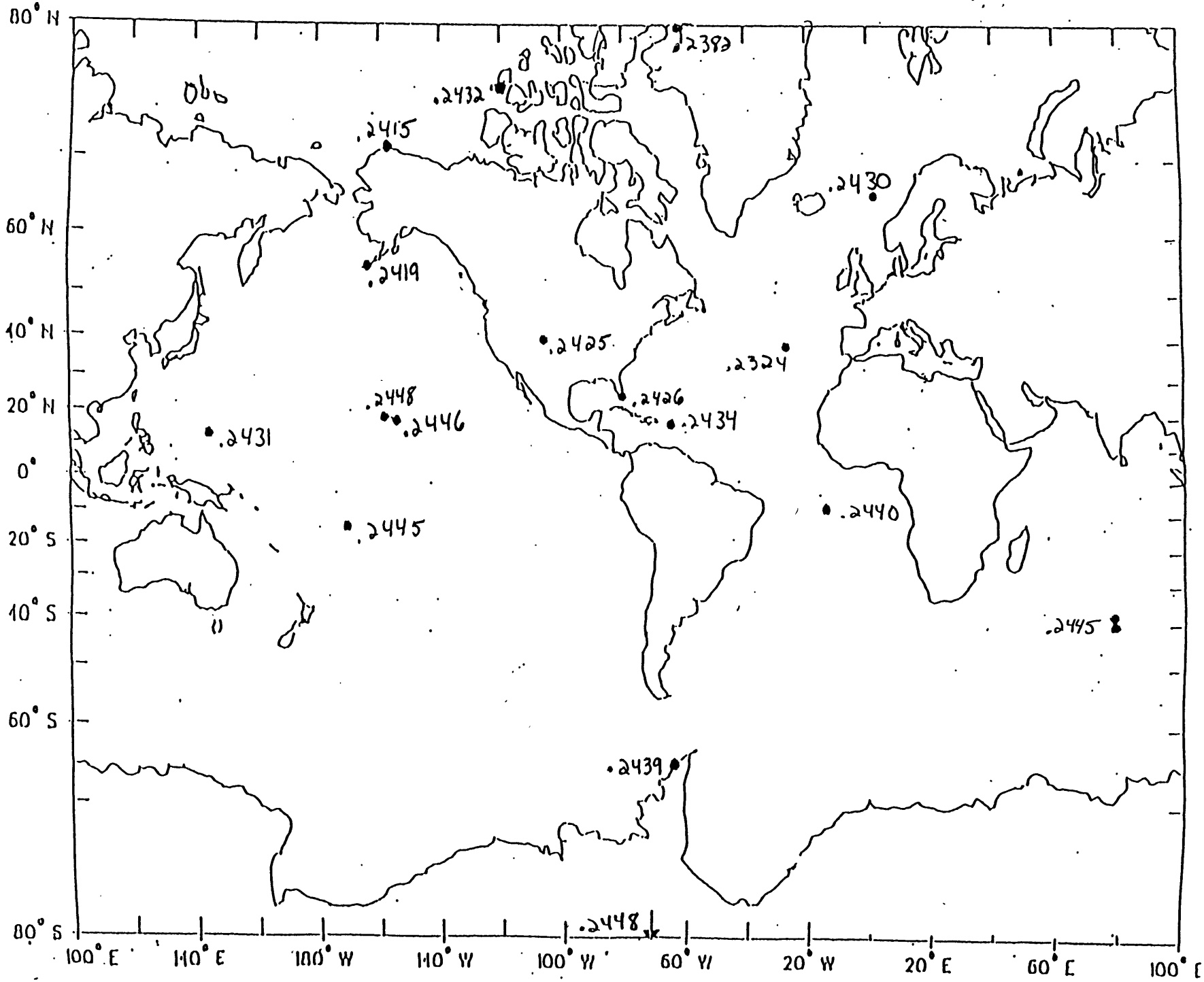

Figure B-15: First Non-Seasonal Eigenvector

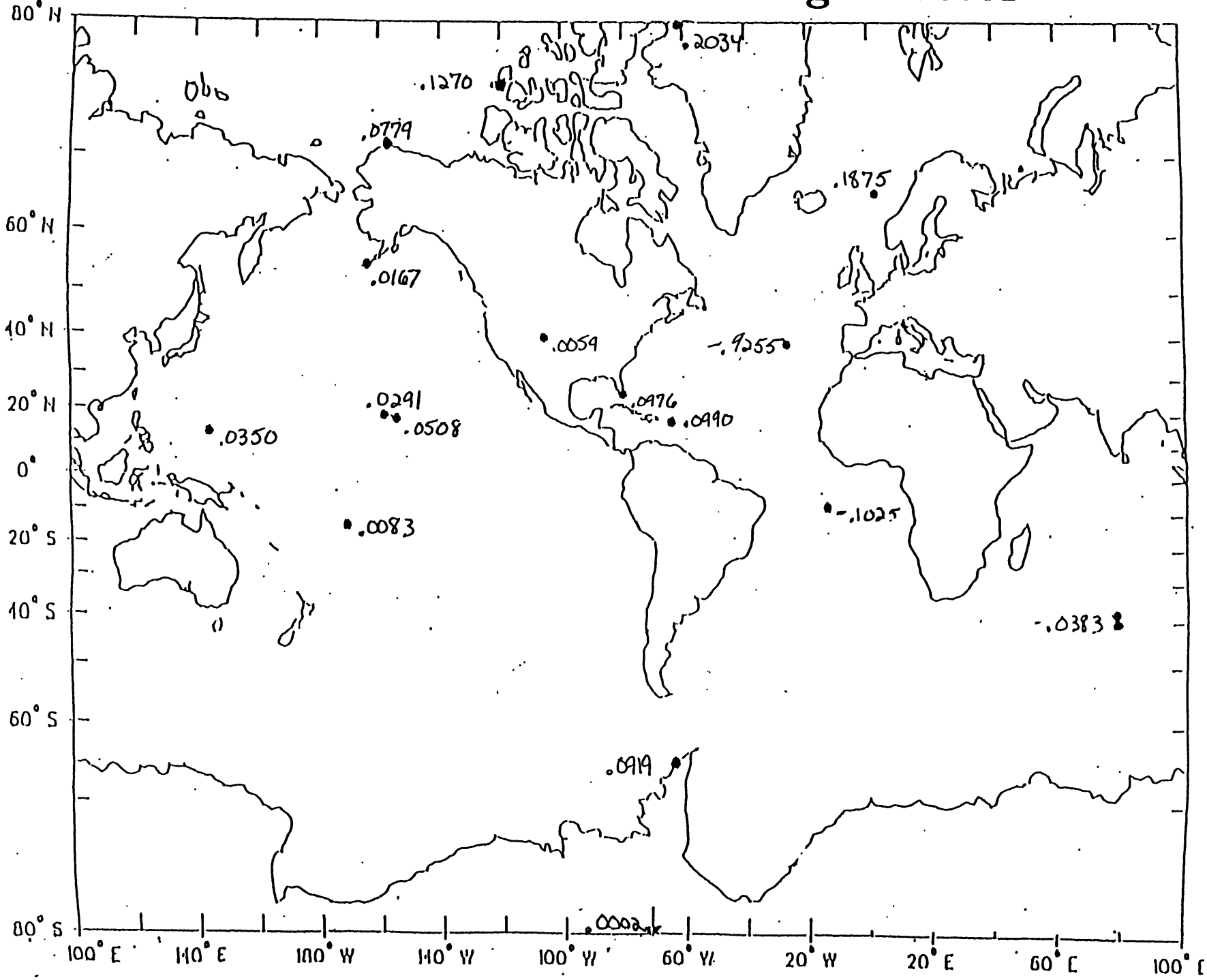

Figure B-16: Second Non-Seasonal Eigenvector

Third Non-Seasonal Eigenvector

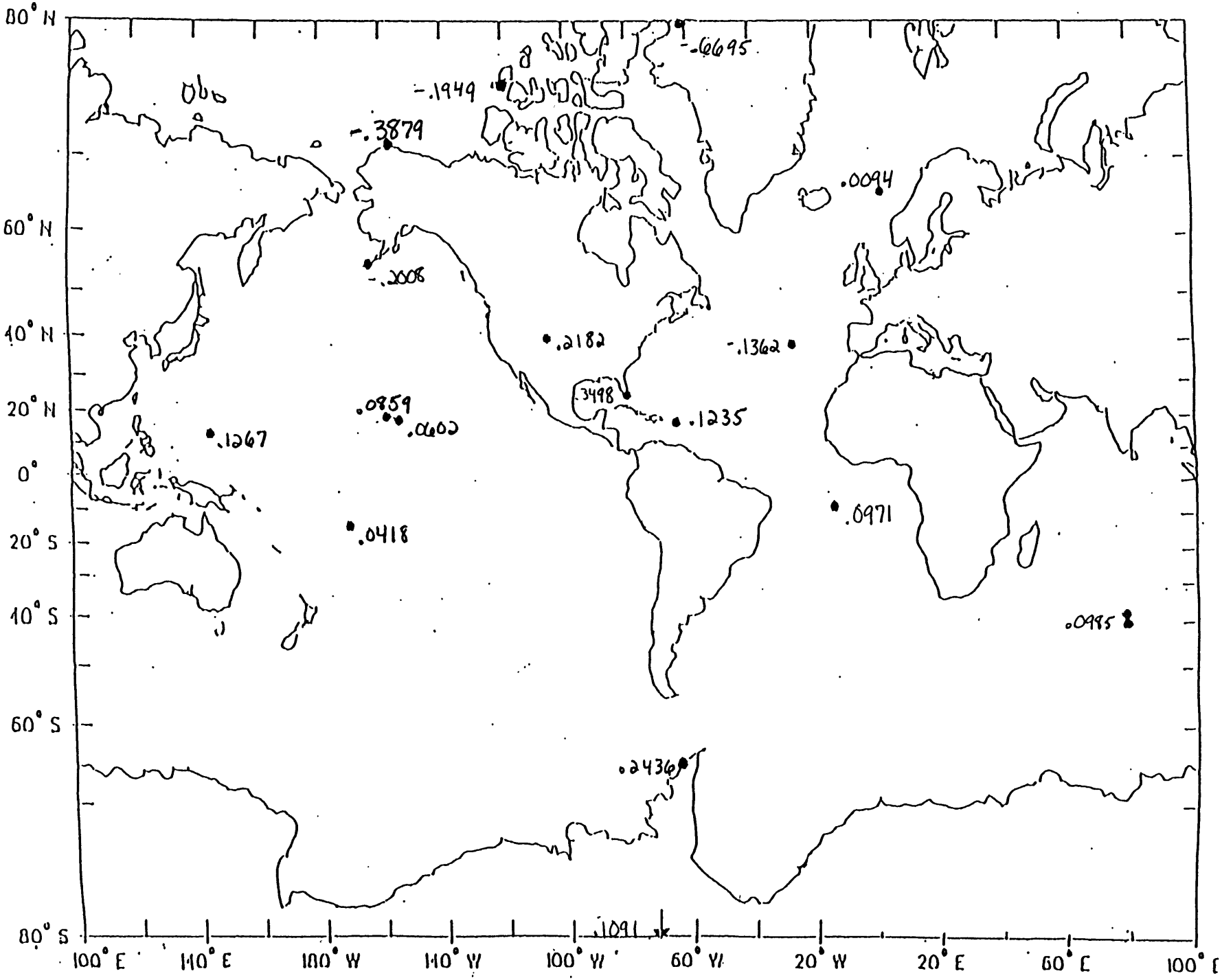

Figure B-17: Third Non-Seasonal Eigenvector

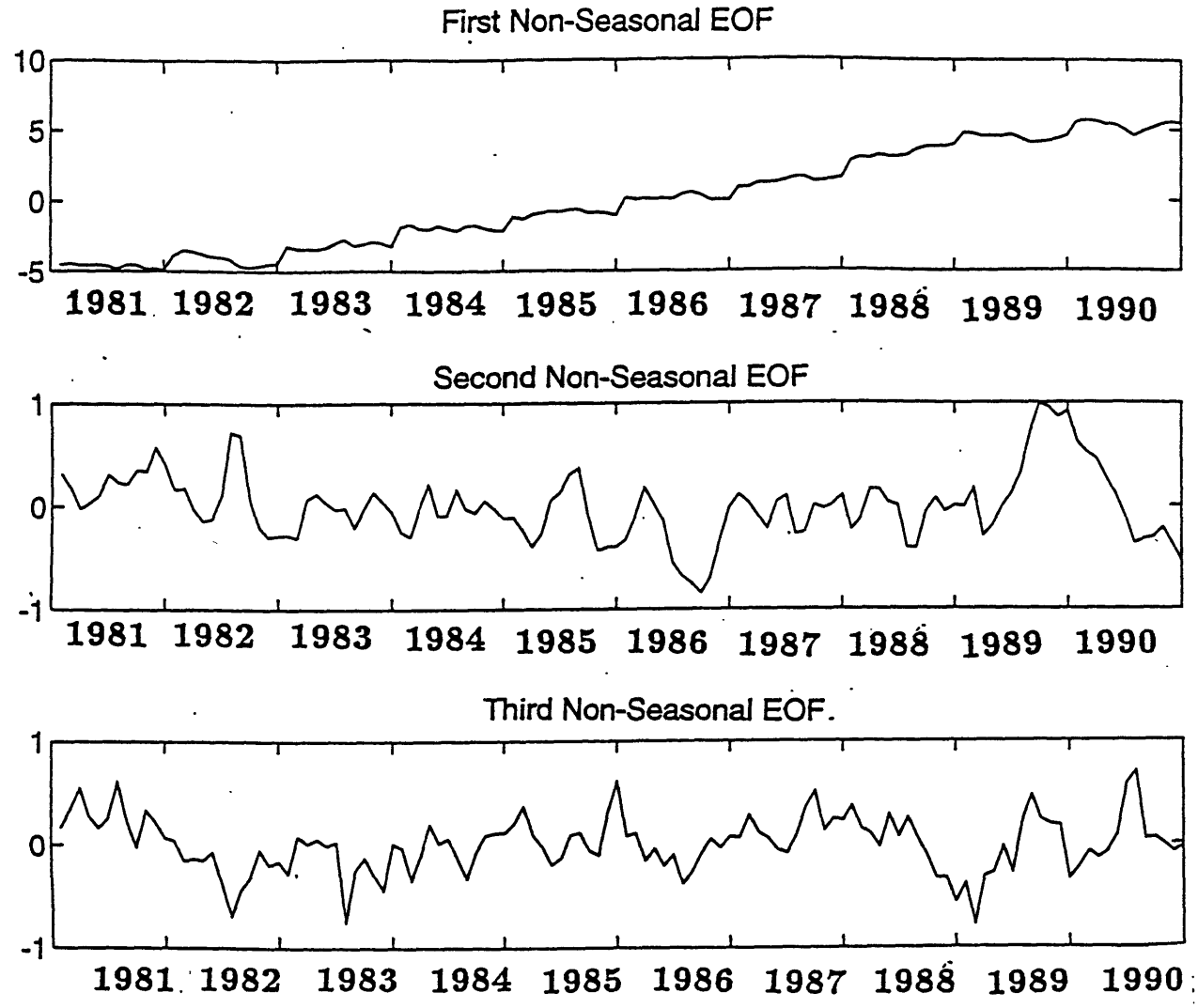

Figure B-18: Northern Hemisphere Non-Seasonal EOF

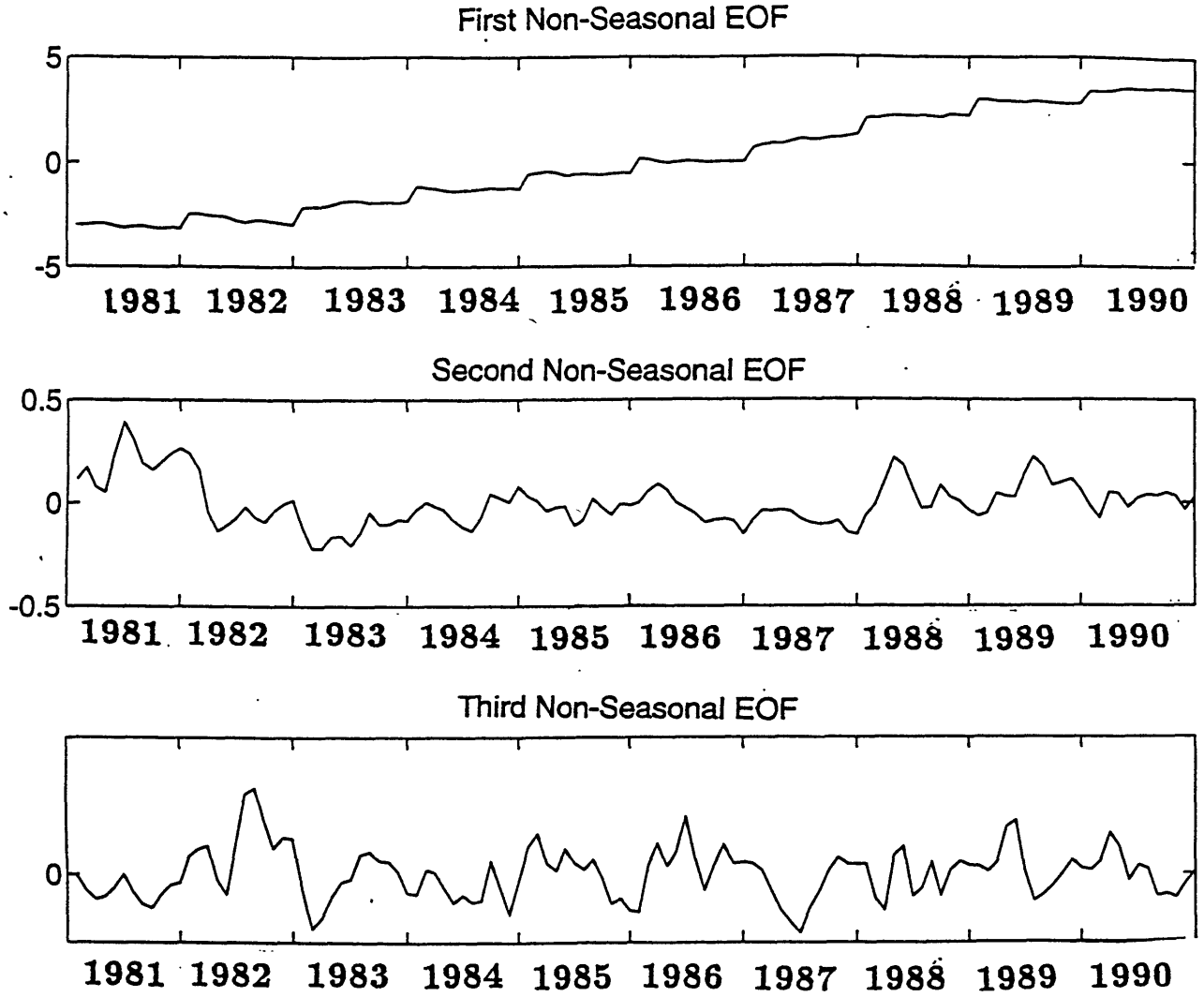

Figure B-19: Southern Hemisphere Non-Seasonal EOF

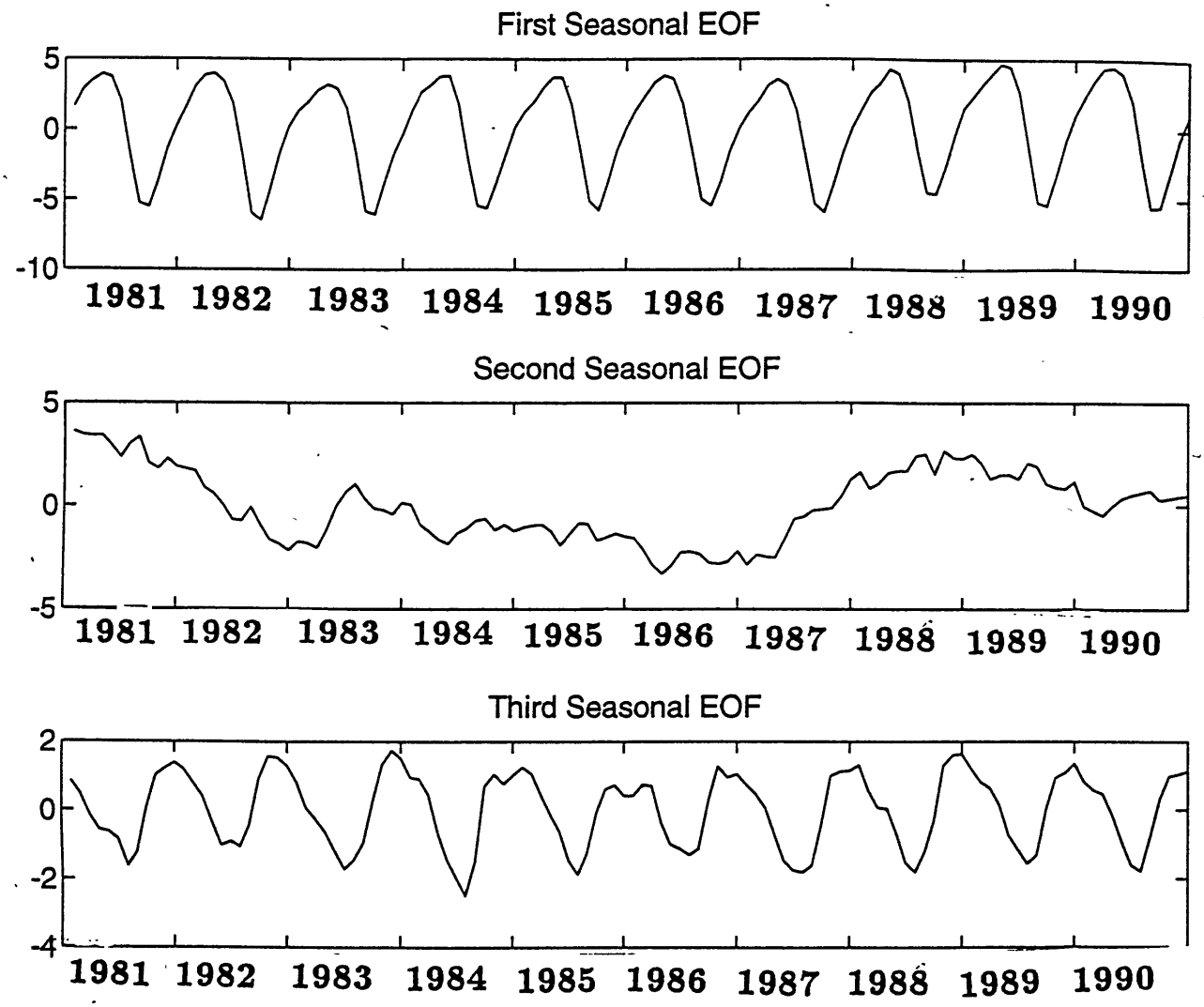

Figure B-20: Seasonal EOF (w/curve-fit)

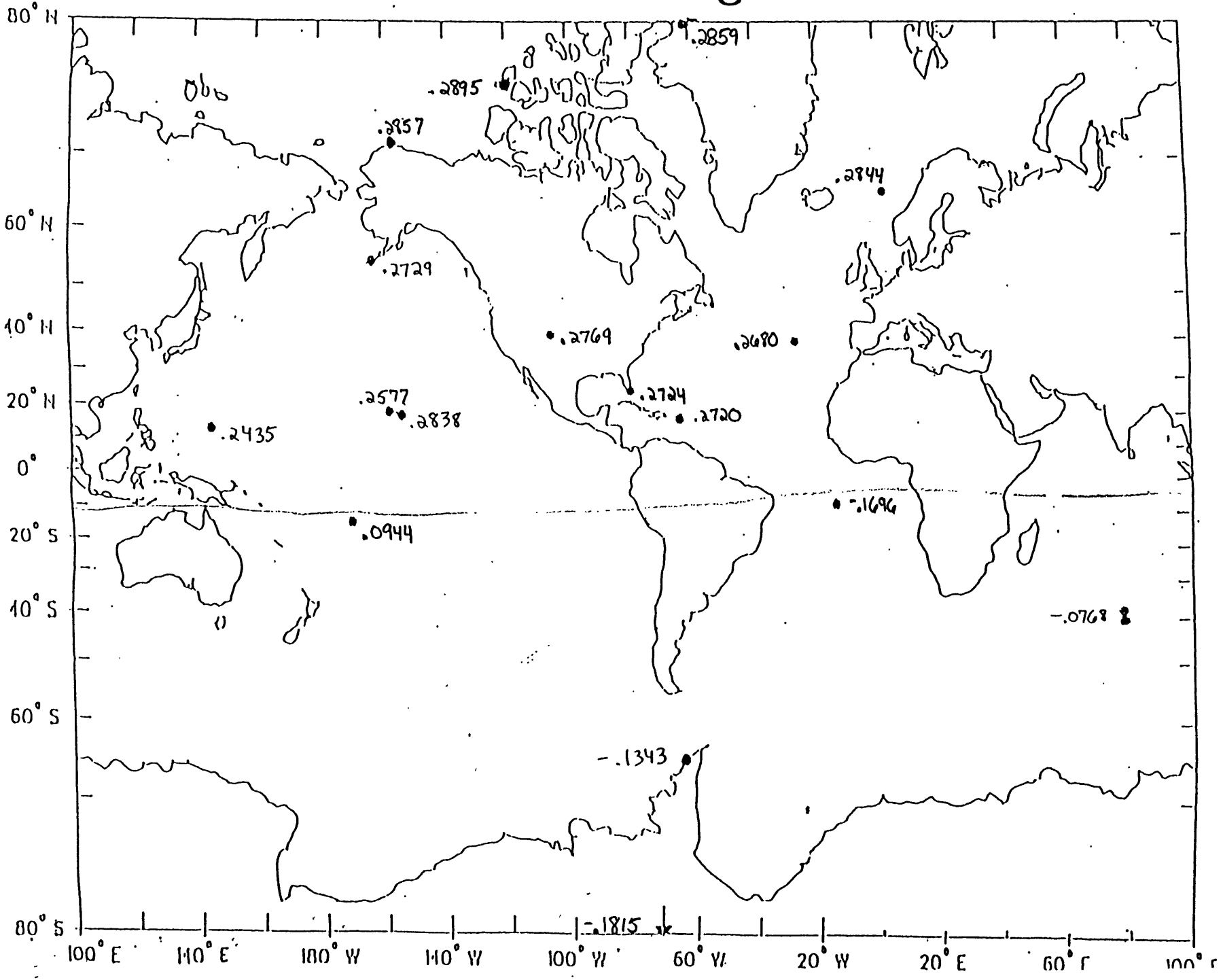

Figure B-21: First Seasonal Eigenvector (w/curve-fit)

Second Seasonal Eigenvector

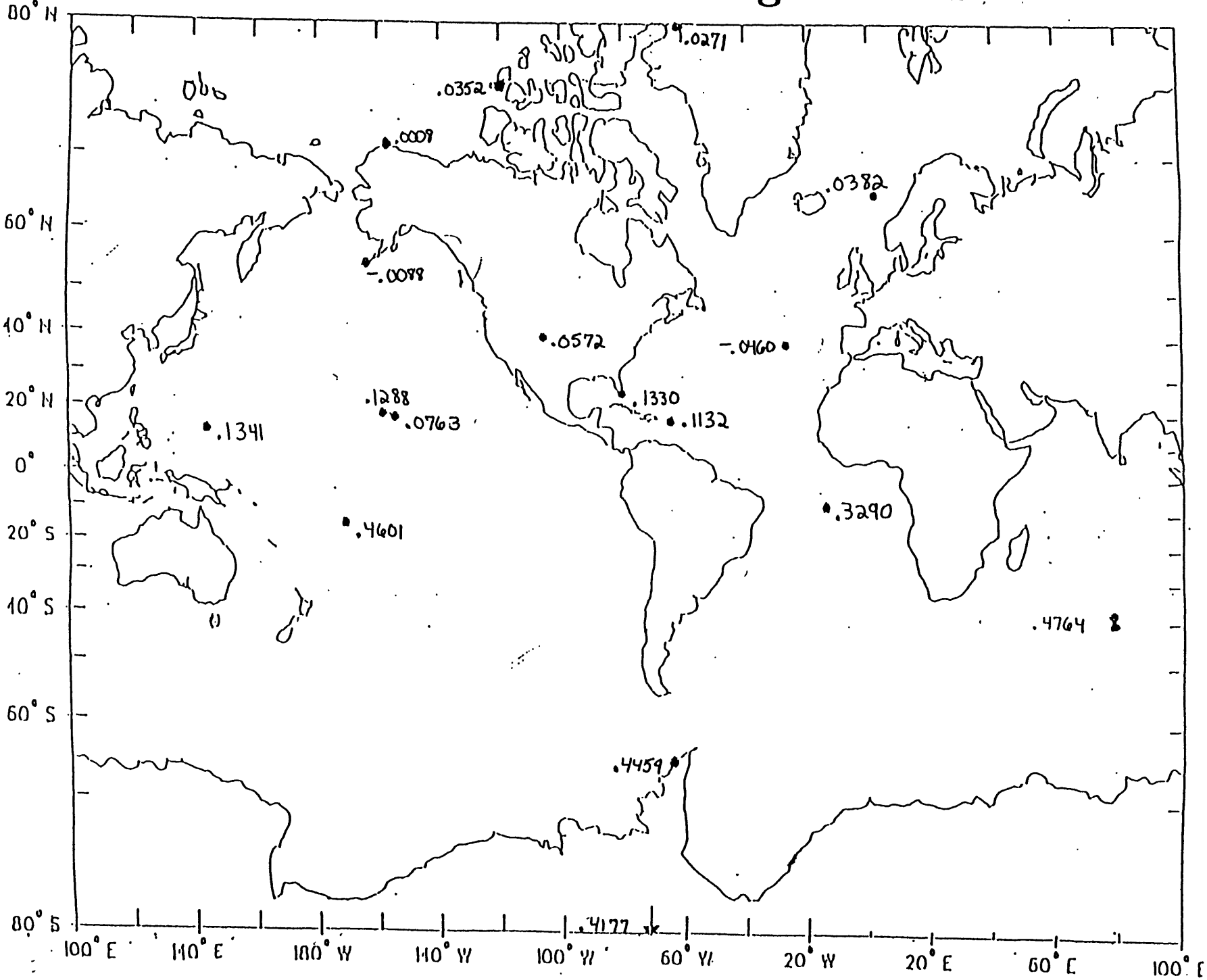

Figure B-22: Second Seasonal Eigenvector (w/curve-fit)

Third Seasonal Eigenvector

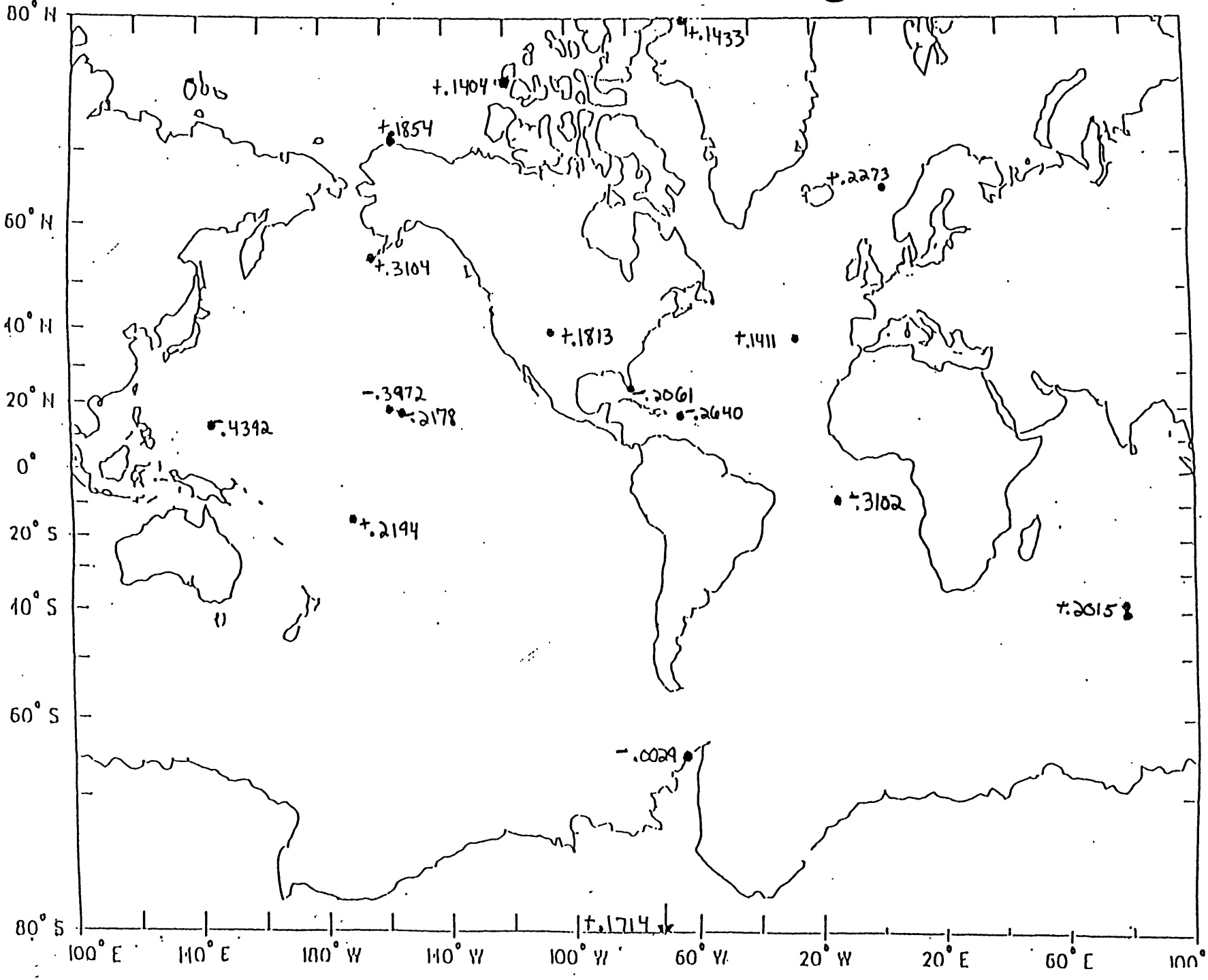

Figure B-23: Third Seasonal Eigenvector (w/curve-fit)

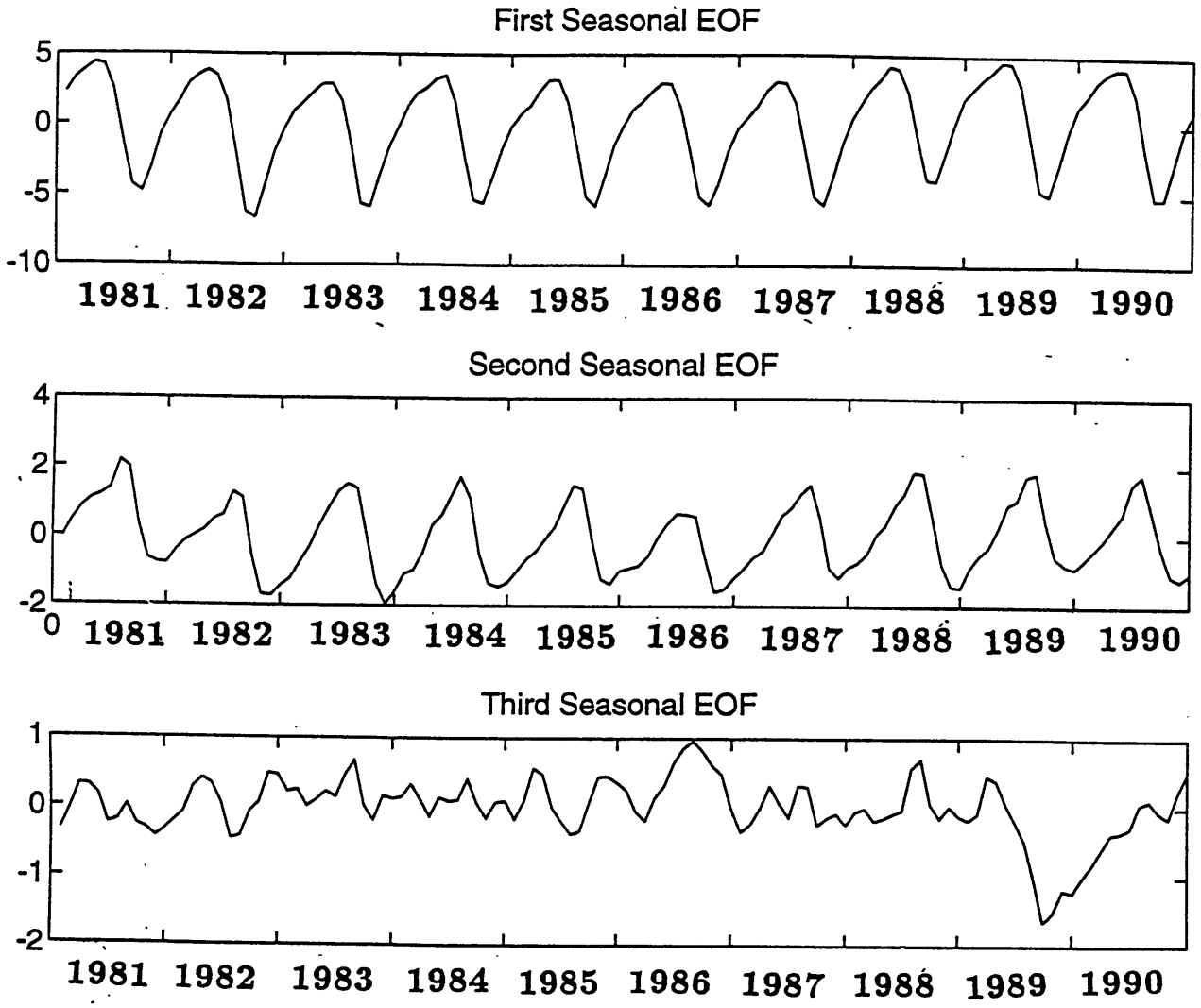

Figure B-24: Northern Hemisphere Seasonal EOF (w/curve-fit)

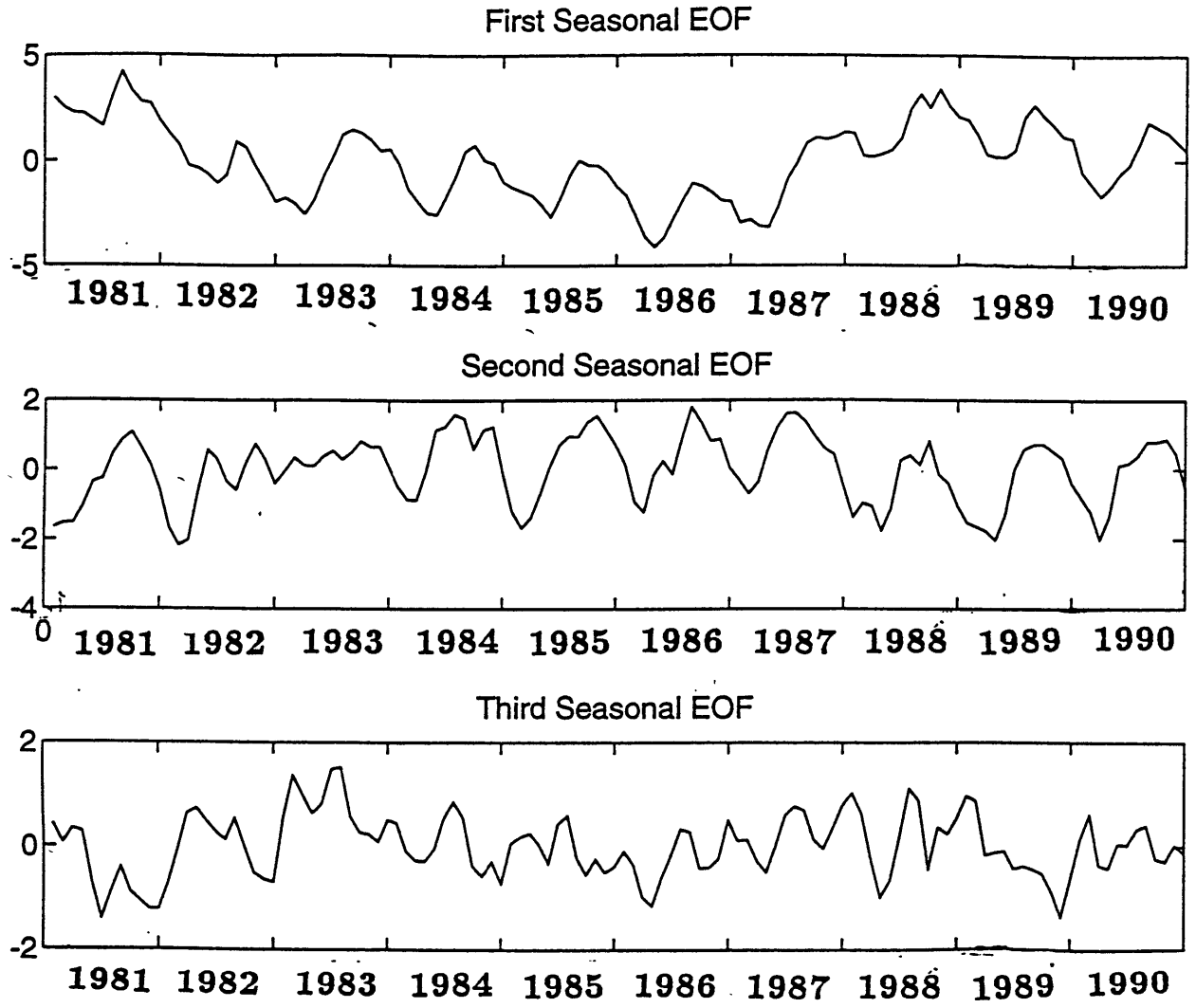

Figure B-25: Southern Hemisphere Seasonal EOF (w/curve-fit)

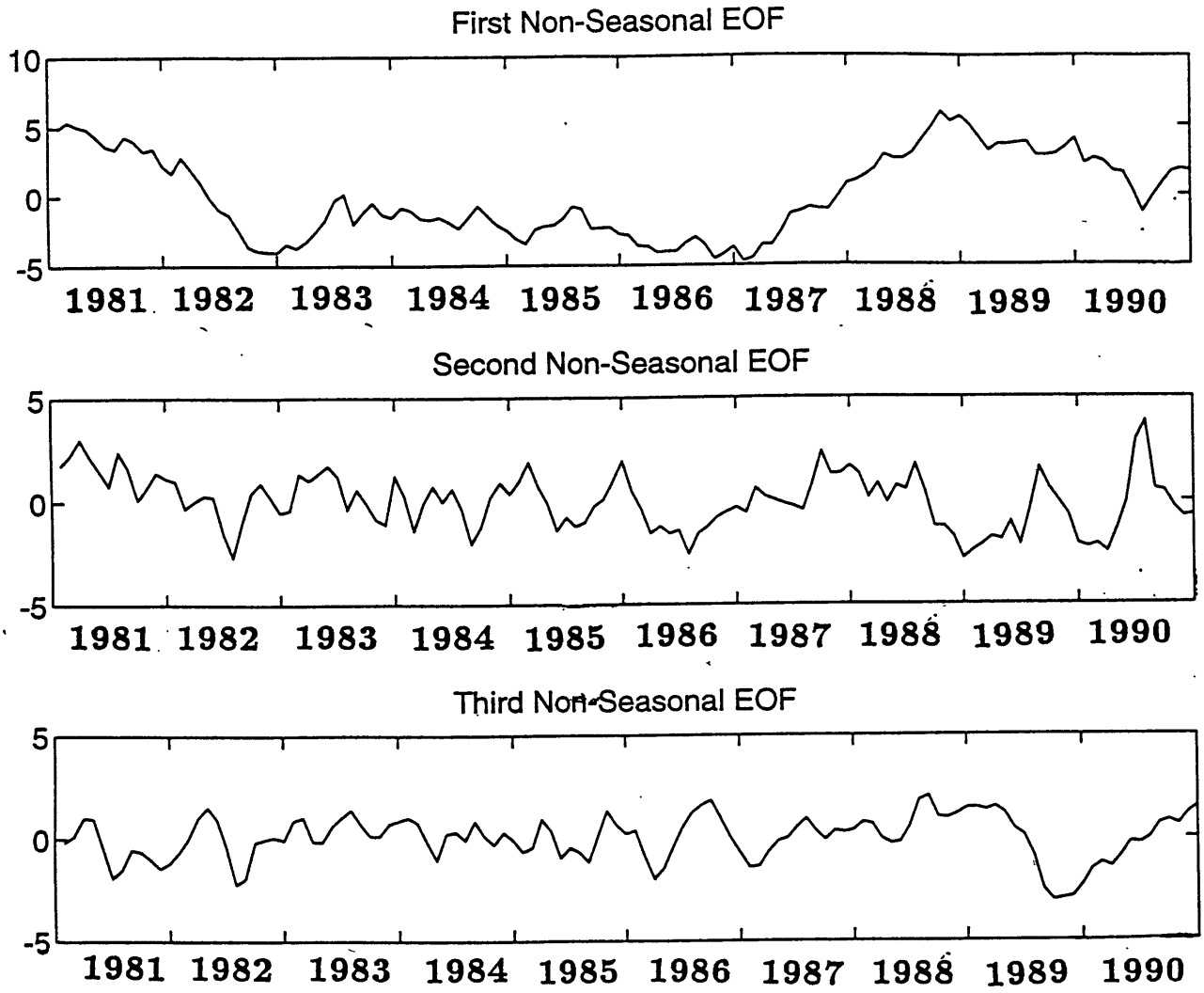

Figure B-26: Non-Seasonal EOF (w/curve-fit)

First Non-Seasonal Eigenvector

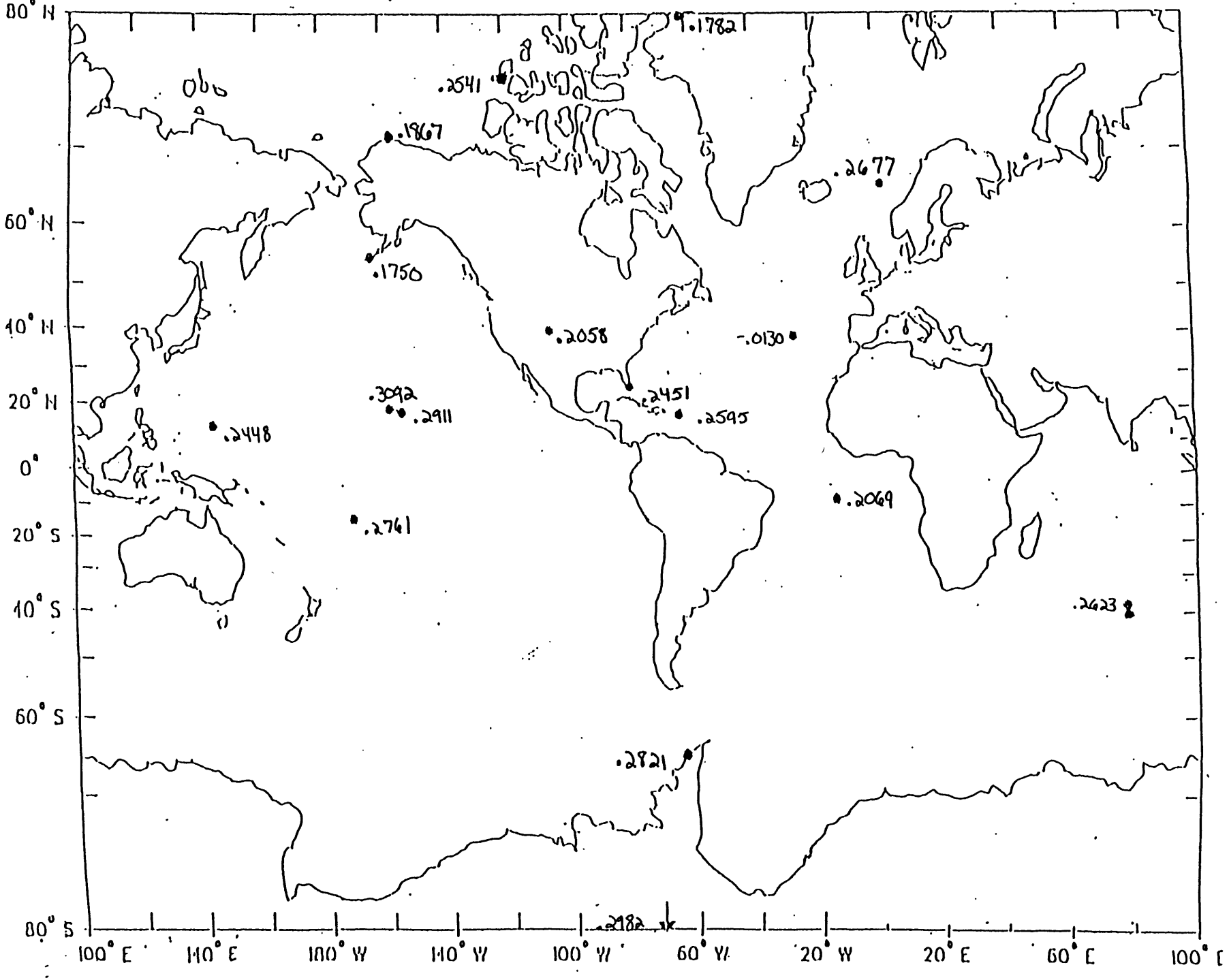

Figure B-27: First Non-Seasonal Eigenvector (w/curve-fit)

Second Non-Seasonal Eigenvector

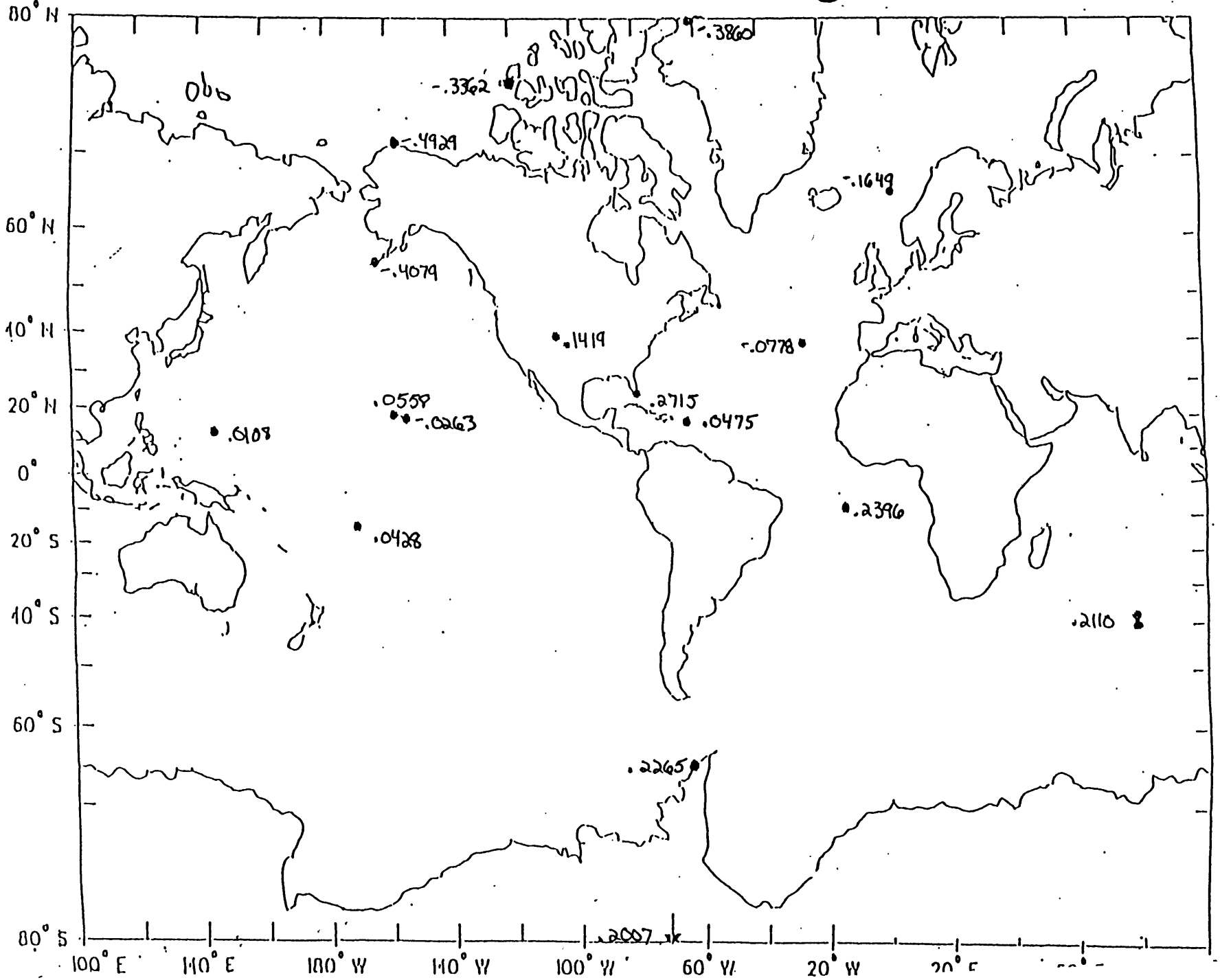

Figure B-28: Second Non-Seasonal Eigenvector (w/curve-fit)

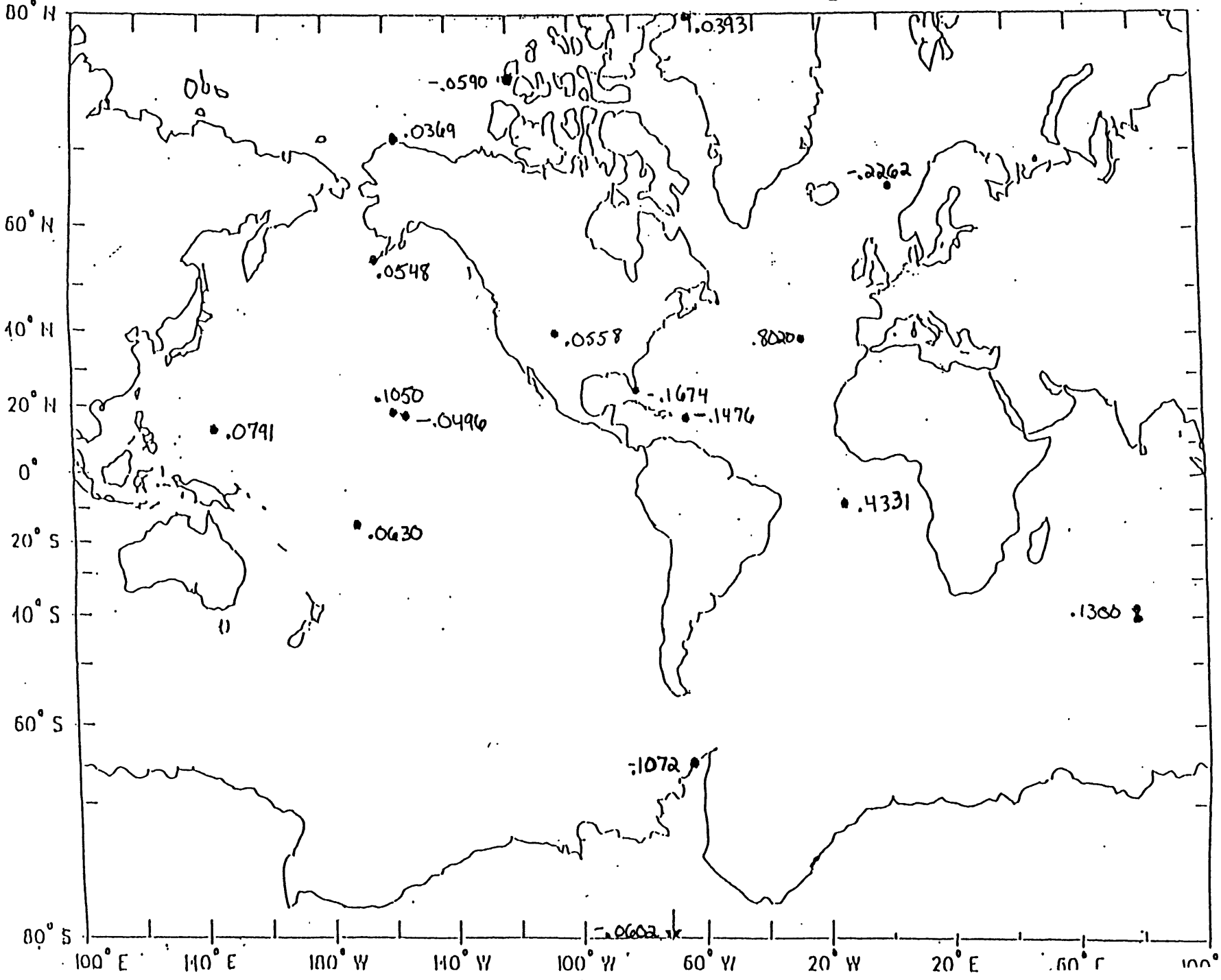

Figure B-29: Third Non-Seasonal Eigenvector (w/curve-fit)

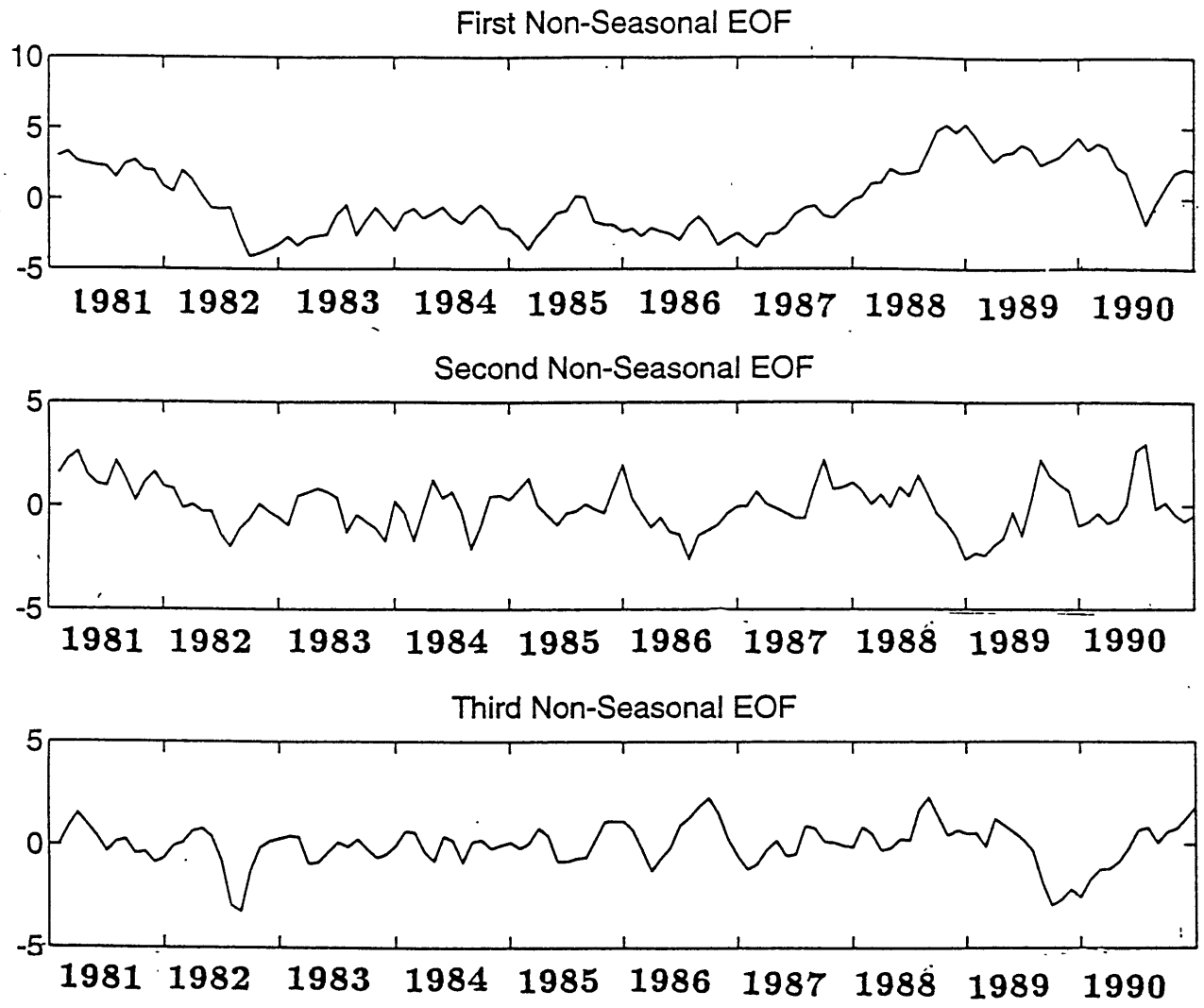

Figure B-30: Northern Hemisphere Non-Seasonal EOF (w/curve-fit)

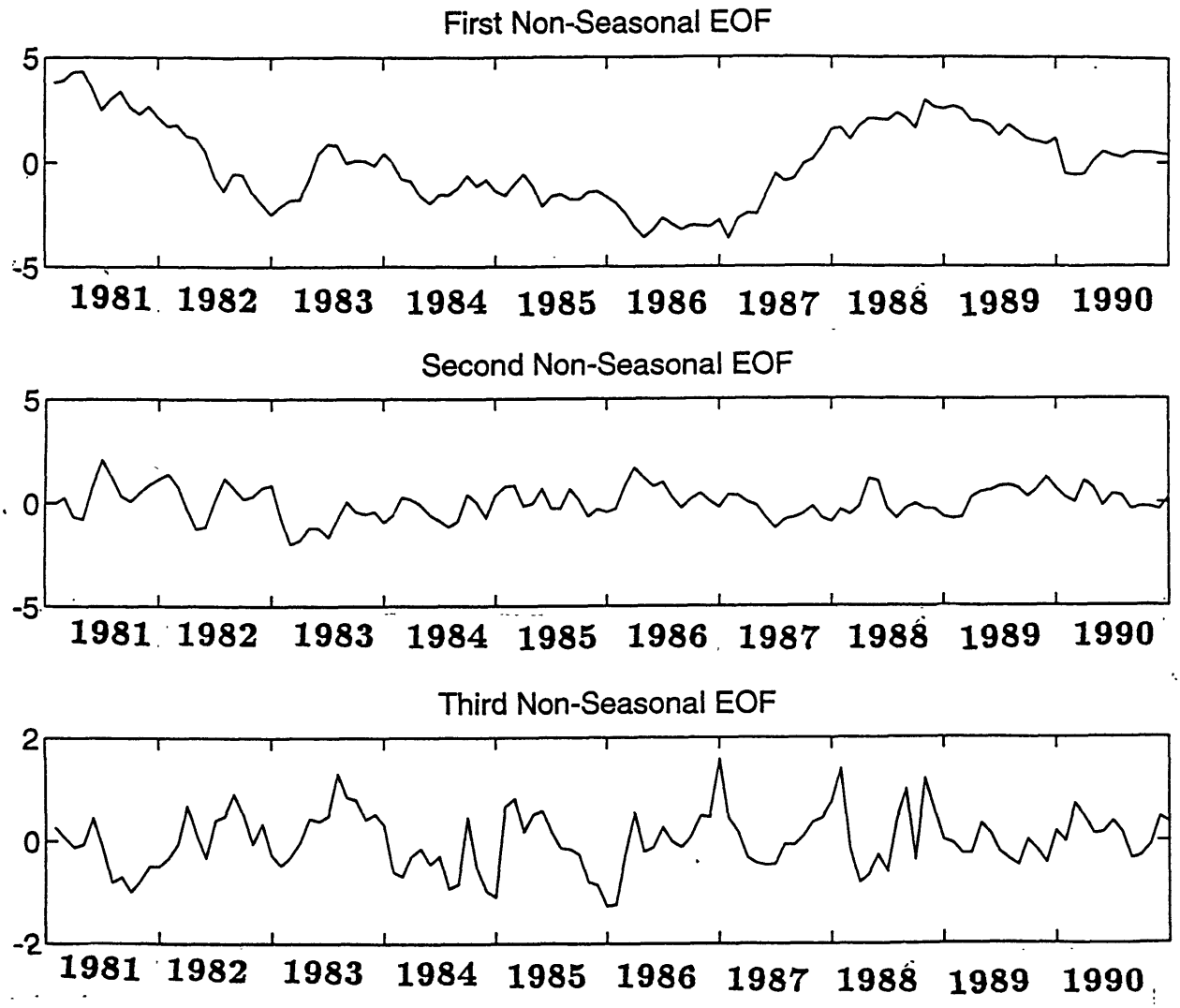

Figure B-31: Southern Hemisphere Non-Seasonal EOF (w/curve-fit)

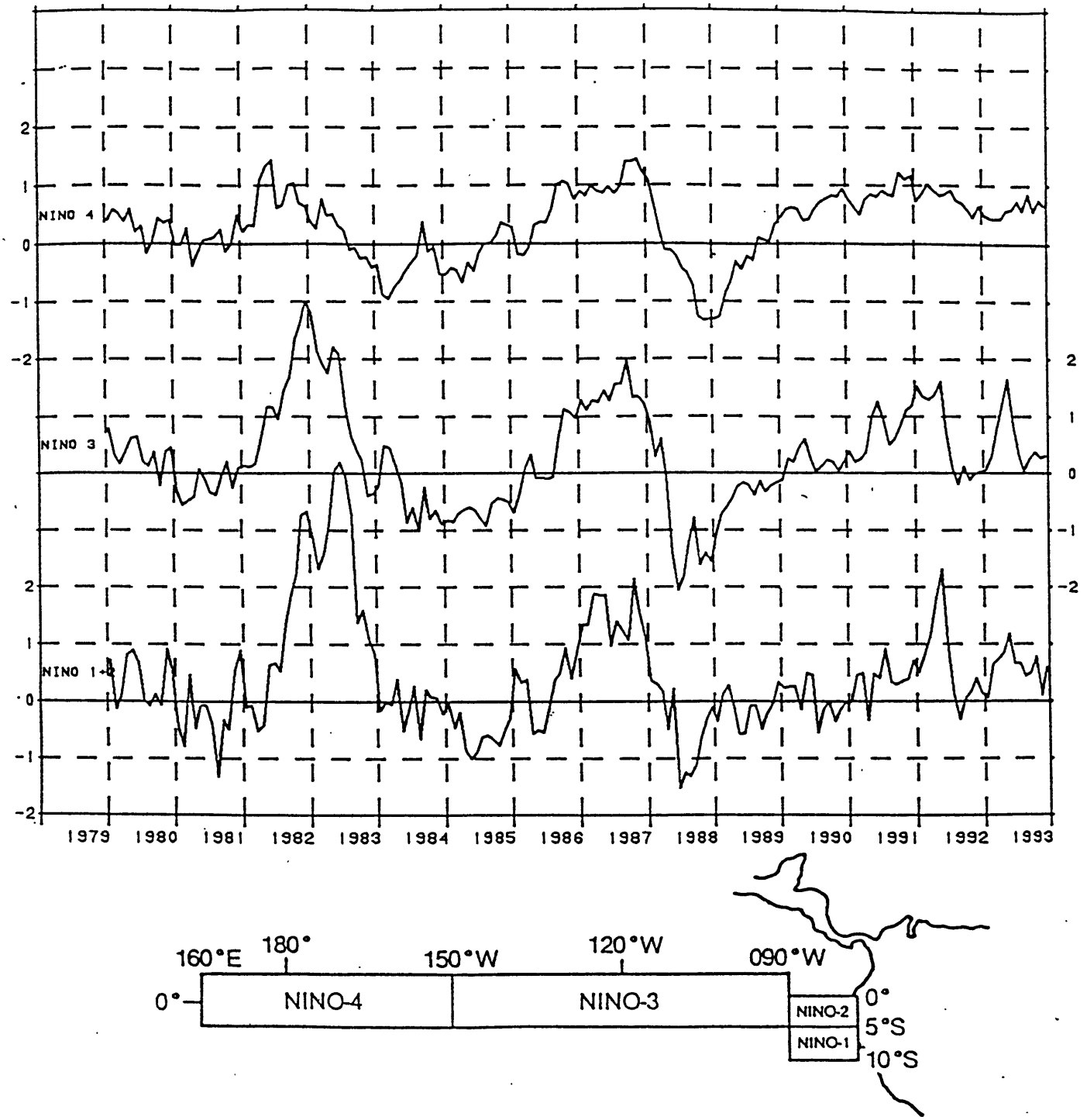

Figure B-32: Equatorial Pacific sea surface temperature anomaly indices (°C) for the areas indicated in the figure. Niño 1+2 is the average over the Niño 1 and Niño 2 areas. Anomalies are computed with respect to the COADS/ICE climatology (Reynolds 1988, *J. Climate*, 1, 75-86). [4]

Bibliography

[1] Bach, W. Crane, A.J., Berger, A.L. & Longhetto, A., *Carbon Dioxide: Current Views and Developments in Energy/Climate Research*, D. Reidel Publishing Co: Dordrecht, Holland (1983).

[2] Bolin, B. & Keeling, C.D., *Large-Scale Atmospheric Mixing As Deduced from the Seasonal and Meridional Variations of Carbon Dioxide*, JGR Vol.68 No.13, 3899-3920 (1963).

[3] Broecker, W.S. & Peng T., *Interhemispheric Transport of Carbon Dioxide by Ocean Circulation*, Nature Vol.356, 587-589 (1992).

[4] *Climate Diagnostics Bulletin: December 1993*, Climate Analysis Center, Washington D.C. (1994).

[5] Gill, Adrian *Atmosphere-Ocean Dynamics*, Academic Press, Inc., San Diego, CA (1982).

[6] Essenwanger, O., *Developments in Atmospheric Science 4A*, Am. Elsevier Publishing Co: NY, NY (1976).

[7] Hoffman, Ross M., *A computer program which calculates radiative fluxes and heating rates in model atmospheres.*, Scientific Report #4 for the study of Climatic Fluctuation Volcanic Aerosol and Carbon Dioxide Changes, Department of Meteorology and Physical Oceanography, MIT, Cambridge, MA (1981).

[8] Hsiung-Wojcik, Jane, *Large Scale Sea-Air Energy Fluxes and Global Sea Surface Temperature Fluctuations*, MIT, Cambridge, MA (1983).

[9] Hu, W., Newell, R.E., & Wu, Z., *Modes of Variability of Global sea Surface Temperature, Free Atmosphere Temperature and Oceanic Surface Energy Flux*, MIT, Cambridge, MA (1993).

[10] Inoue, H. & Sugimura, Y., *Distribution and variations of oceanic carbon dioxide in the western North Pacific, eastern Indian, and Southern Ocean south of Australia.*, Tellus, Vol.40B, 308-320 (1988).

[11] Inoue, H., Sugimura, Y. & Fushimi, K., *pCO_2 and $\delta^{13}C$ in the air and surface sea water in the western North Pacific.*, Tellus, Vol.39B, 228-242 (1987).

[12] Leutwyler, Kristin, *No Global Warming?*, Sci. Am., (1994).

[13] Newell, R.E., Vincent, D.G. & Kidson, J.W., *Interhemispheric mass exchange from meteorological and trace substance observations.*, Tellus, Vol.21 No.5, 641-647 (1968).

[14] Newell, R.E., Navato, A.R., & Hsuing, J., *Long-term Global Sea Surface Temperature Fluctuations and their Possible Influence on Atmospheric CO_2 Concentrations*, Pageoph. Vol.116, 351-370 (1978).

[15] Peixoto, Josè P. & Oort, Abraham H., *Physics of Climate*, American Institute of Physics, NY, NY (1992)

[16] Prinn, Ronald G., *Global Budgets for the Greenhouse Gases*, MIT, Cambridge, MA (1991).

[17] *Provisional Daily Atmospheric Carbon Dioxide Concentrations*, World Meteorological Organization, No. 1986

[18] Riebesell, U., Wolf-Gladrow, D.A., & Smetacek, V., *Carbon Dioxide Limitation of Marine Phytoplankton Growth Rates*, Nature 361, 249-251 (1993).

[19] Sarmiento, J.L., *Atmospheric CO_2 Stalled*, Nature Vol.365, 697-698 (1993).

[20] Sarmiento, J.L. & Sundquist, E.T., *Revised Budget for the Oceanic Uptake of Anthropogenic Carbon Dioxide*, Nature Vol.356, 589-592 (1992).

[21] Siegenthaler, U. & Sarmiento, J.L., *Atmospheric Carbon Dioxide and the Ocean*, Nature Vol.365, 119-125 (1993).

[22] Strang, Gilbert, *Linear Algebra and Its Applications, Third Edition*, San Diego, CA (1986).

[23] Tans, P.P., Fung, I.Y., Takahashi, T., *Observational Constraints on the Global Atmospheric CO_2 Budget*, Science Vol.247, 1431-1438 (1990).

[24] Taylor, John, *The Mutable Carbon Sink*, Nature Vol.366, 515-516 (1993).

[25] *Trends '91*, Carbon Dioxide Information Analysis Center, Oak Ridge National Laboratory, Oak Ridge, TN (1991).

[26] Verstraete, Michel M., *Empirical Orthogonal Functions: the method and its applications.*, MIT, Cambridge, MA (1978).

[27] Watson, Andrew, *Conveying That Sinking Feeling*, Nature Vol.356, 561-562 (1992).

[28] Weiss, Jahnke, R.A., & Keeling, C.D., *Seasonal Effects of Temperature and Salinity on the Partial Pressure of CO_2 in Seawater*, Nature Vol.300, 511-513 (1982).

MASSACHUSETTS INSTITUTE OF TECHNOLOGY
CAMBRIDGE, MASSACHUSETTS 02139
U.S.A.

(617) 253-2195

GRADUATE STUDENT COUNCIL
WALKER MEMORIAL
ROOM 50-222

18 May 1994

Dear Graduate Administrator,

As in previous years, the GSC is planning a comprehensive series of orientation events for incoming graduate students this fall. In the interest of coordinating our own activities with those planned by individual departments, we have included a tentative schedule of GSC organized events.

We would be very grateful if you would send a copy of your own orientation schedule to us. Once we have received copies of all the department schedules we will attempt to adjust ours to minimize conflicts.

We look forward to working with you in making Orientation an enjoyable experience for the incoming graduate students,

Sincerely,

Joe Bambenek
Co Chair, GSC Orientation Committee

David Bombard
Co Chair, GSC Orientation Committee

Chris Gittins
Co Chair, GSC Orientation Committee

Roger Kermode
President, GSC

enclosure